BeFo
STIFTELSEN BERGTEKNISK FORSKNING
ROCK ENGINEERING RESEARCH FOUNDATION

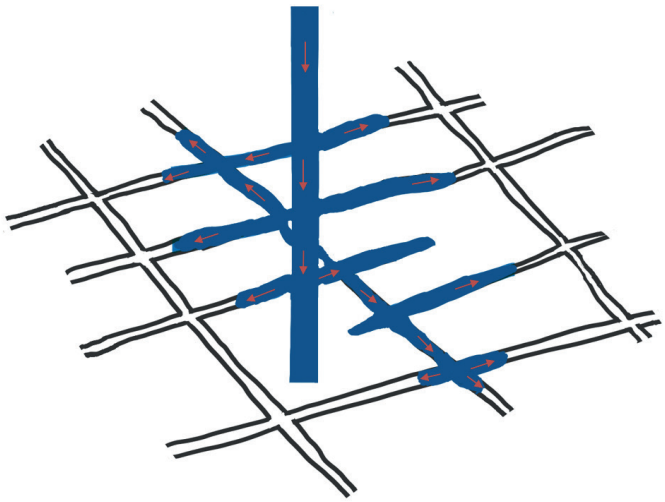

ANALYSIS OF CEMENT GROUT PROPAGATION IN FRACTURED ROCKS

Liangchao Zou
Ulf Håkansson
Vladimir Cvetkovic

BeFo Report 200

STIFTELSEN BERGTEKNISK FORSKNING
ROCK ENGINEERING RESEARCH FOUNDATION

ANALYSIS OF CEMENT GROUT PROPAGATION IN FRACTURED ROCKS

Analys och simulering av cementinjektering i sprickigt berg

Liangchao Zou, KTH Royal Institute of Technology

Ulf Håkansson, Skanska Sweden AB.

Vladimir Cvetkovic, KTH Royal Institute of Technology

BeFo Report 200
Stockholm 2021
ISSN 1104-1773
ISRN BEFO-R-200-SE

PREFACE

Although a simplification of the real world, analytical solutions play an important role in modelling of flow of grouts in jointed rock. Two analytical solutions for 2D radial flow of a Bingham fluid between smooth parallel plates are currently being used, both with simplifying assumptions (El Tani, 2012, Gustafson et al, 2013; Zou et al, 2020).

The main objective of the present study has been to assess which of the two solutions is correct and thereby recommended for use in the grouting community. The solution used in this study assumes a constant plug flow region, similar to 1D flow in channels and pipes, in order to fulfil the requirement of mass balance (Eq. of continuity).

The other available solution (Dai & Bird, 1981; Hässler, 1991, Gustafson et al, 2013; Hoang et al, 2021) implies a radius dependent plug flow region and in order to fulfil mass balance introduces a vertical velocity component (e.g. Hoang et al, 2021).

One cannot conclude from the current work that one solution is right and the other wrong. They are both simplifications and it is interesting to note that for practical purposes, e.g. for grouting simulations, it does not matter which one you use as they both generate similar results. However, it should be stressed that the solution presented in this study has simpler mathematical expressions that makes it easier to use by practitioners involved in grouting.

This study also introduces numerical simulations, as a complement to the analytical solutions, in order to determine the effect of rough fractures, water filled fractures, channel networks and rheological properties of the used grout.

The research presented in this report was mainly carried out at the Department of Sustainable Development, Environmental Sciences and Engineering (SEED), at KTH Royal Institute of Technology. The work was supervised by Prof. Vladimir Cvetkovic, KTH, and Dr. Ulf Håkansson, Skanska Sweden AB. Their support, encouragement, and valuable insights of the work are greatly appreciated.

The input from the project reference group is also gratefully acknowledged. The following have participated:

Thomas Dalmalm and Christian Butron (Swedish Transport Administration), Ann Emmelin och Mikael Creütz (Golder), Magnus Zetterlund (Norconsult), Patrik Vidstrand (SKB), Tommy Ellison (Besab), Johan Wiklund (Incipientus) and Per Tengborg (BeFo).

Stockholm, August 2021

Per Tengborg

FÖRORD

Även om det är en förenkling av den verkliga världen spelar analytiska lösningar en viktig roll vid modellering av flödet av injekteringsmedel i sprickigt berg. Två analytiska lösningar för 2D-radiellt flöde av en Binghamvätska mellan släta parallella plattor används för närvarande, båda med förenklande antaganden (El Tani, 2012, Gustafson m.fl. 2013; Zou et al, 2020).

Syftet med denna studie har varit att bedöma vilken av de två lösningarna som är korrekt och som därmed kan rekommenderas för användning vid praktisk injektering. Den lösning som används i denna studie förutsätter en konstant plug i radiell riktning vid en viss inträngning, liknande 1D-flöde i kanaler och rör, för att uppfylla kravet på massbalans (kontinuitet).

Den andra tillgängliga lösningen (Dai & Bird, 1981; Hässler, 1991, Gustafson m.fl. 2013; Hoang et al, 2021) innebär en radieberoende plug och för att uppfylla massbalansen införs en vertikal hastighetskomponent (t.ex. Hoang et al., 2021).

Man kan inte dra slutsatsen av detta arbete att den ena lösningen är rätt och den andra fel. De är båda förenklingar och det är intressant att notera att för praktiska ändamål, t.ex. för simuleringar av injektering, spelar det ingen roll vilken man använder eftersom de båda genererar liknande resultat. Det bör dock betonas att den lösning som presenteras i denna studie har mycket enklare matematiska uttryck som gör det lättare att använda av utövare som injekterar.

Denna studie introducerar också numeriska simuleringar, som ett komplement till de analytiska lösningarna, för att bestämma effekten av rå sprickor, vattenfyllda sprickor, kanalnätverk och reologiska egenskaper hos det använda injekteringsbruket.

Forskningen som presenteras i denna rapport har främst utförts på Institutionen för hållbar utveckling, miljövetenskap och teknik (SEED) på KTH.
Arbetet har handletts av Professor Vladimr Cvetkovic, KTH och Dr. Ulf Håkansson, Skanska Sverige AB. Deras stöd, uppmuntran och värdefulla insikter är mycket uppskattat.

Ett stort tack riktas också till projektets referensgrupp där följande personer har ingått: Thomas Dalmalm och Christian Butron (Trafikverket), Ann Emmelin och Mikael Creütz (Golder), Magnus Zetterlund (Norconsult), Patrik Vidstrand (SKB), Tommy Ellison (Besab), Johan Wiklund (Incipientus) och Per Tengborg (BeFo).

Stockholm, augusti 2021
Per Tengborg

ACKNOWLEDGEMENT

The BeFo Rock Engineering Research Foundation, Sweden (grant number 392) is gratefully acknowledged for the financial support to this study.

We would like to thank the reference group for this project for their valuable comments and constructive suggestions during the project reference group meetings. The reference group members are Thomas Dalmalm and Christian Butron from the Swedish Transport Administration, Ann Emmelin and Mikael Creütz from Golder, Magnus Zetterlund from Norconsult, Patrik Vidstarnd from SKB, Tommy Ellison from Besab, Johan Wiklund from Incipientus and Per Tengborg from BeFo.

We also would like to thank Håkan Stille, Lars Hässler, Johan Claesson, Johan Funehag, Mashuqur Rahman and John Shamu for their helpful discussion.

SUMMARY

Modeling of cement grout propagation in fractured rocks is important for the design, execution and monitoring of rock grouting in practice. In this project, we studied non-Newtonian cement grouts propagation in rock fractures by theoretical analyses and numerical simulations.

The analytical solutions for radial flow of a Bingham fluid, between parallel plates, are analyzed and existing disagreements in the literature regarding the two different analytical solutions that are used for analysis of grouting in rock fractures is investigated. The analyses reveal that the two solutions are both zero-order approximation solutions based on different assumptions, that is *with* or *without* consideration of the vertical velocity component across the aperture. The one without considering the vertical velocity yields to a solution with radius-independent plug flow region, which largely simplifies the calculations. By using the solution with radius-independent plug flow region, Bingham grout penetration and flowrate (at the injection borehole) evolution as functions of grouting time are given for the first time. Discrepancies in the two approximation solutions for grout penetration and flowrate evolution are illustrated, showing negligible differences. The clarification of the plug flow region and evaluation of discrepancies in the two solutions presented in this work improves our confidence and simplifies modeling and design of grouting in rock engineering applications.

In reality, rock fracture grouting process involves non-Newtonian fluid flow in fractures with rough surfaces, which is rarely studied in the literature. To investigate the impact of fracture surface roughness on rock fracture grouting, we presented direct numerical simulations of non-Newtonian grouts flow in single rough-walled fractures, using a regularized method (i.e., the Bingham-Papanastasiou model) to approximate the yield-stress. The rough-walled rock fracture models are created from a laser-scanned surface of a granite rock sample, to represent realistic features of natural rock fractures. The numerical results show nonlinear behaviors of non-Newtonian fluid flow in rough-walled fractures caused by non-Newtonian rheological properties and enhanced by the fracture surface roughness. The surface roughness significantly reduces the effective transmissivity (defined as the ratio between the flowrate and the pressure gradient) when Reynolds number (Re) is relatively large, i.e., Re >10.

A mathematical model based on the Reynolds flow equation for cement grout propagation in a homogeneous water-saturated rock fracture is presented. The model is based on two-phase flow, i.e., grout as a Bingham fluid and groundwater as a Newtonian fluid, and is used for investigating the importance of the water flow in rock grouting. The modeling results for the two-phase flow generally show the importance of the water phase that can significantly affect the pressure distribution and grout propagation in the fracture, especially under the condition of grout hardening. Such effects depend on the viscosity ratio between the grout and groundwater, which becomes increasingly important for cases with smaller values of the viscosity ratio. Applying an analytical solution based on single-

phase flow, i.e., neglecting the impact of groundwater flow, for modeling of rock fracture grouting, will generally overestimate the propagation length.

The two-phase flow model for single fractures is extended to simulate non-Newtonian cement grouts propagation in water-saturated fracture networks. We verified the two-phase flow model by comparing numerical simulation results of two-phase flow of cement grouts propagation in fracture networks with the benchmark data in Håkansson (1987). Using this extended model for numerical simulations on the grout propagation the impacts of network geometry, hydraulic aperture distribution and the rheological properties (yield stress and plastic viscosity) are investigated. Cement grout propagation in randomly generated two-dimensional discrete fracture network (2D DFN) are simulated with different cases of hydraulic aperture variability, i.e., constant aperture, uncorrelated and length-correlated heterogeneous apertures following a truncated lognormal distribution. The results indicate that network structure and hydraulic aperture variability significantly affect the grout propagation negatively in 2D DFN systems. The randomized network structure and uncorrelated heterogeneous apertures significantly delay the propagation rate and largely increase the variability range of the penetration volume fraction (the ratio between penetrated volume and total volume of fractures). In contrast, in the case with length-correlated heterogeneous apertures, the propagation rate increases, while the variability range and rate of change of the penetration volume fraction decreases. The rheological properties of cement grouts, i.e., yield stress and plastic viscosity, also significantly affect cement grouts propagation in fracture networks. The propagation rate in the fracture networks reduces with the increase of the yield stress and the plastic viscosity of the cement grouts. The results presented in this report will be helpful in the design and prediction of rock grouting.

Keywords: rock grouting, Bingham fluid, fracture networks, two-phase flow

SAMMANFATTNING

Modellering av cementbruks spridning i sprickist berg är viktigt för en ökad förståelse vid projektering, utförande och kontroll av injektering i praktiken. I detta projekt studerade vi icke-Newtonsk cementinjektering i bergssprickor genom teoretiska analyser och numeriska simuleringar.

De analytiska lösningarna för radiell strömning av en Bingham vätska studeras kritiskt och tvetydigheter i litteraturen beträffande pluggflödet i de två olika lösningar som används, för analys och design av injektering i bergssprickor, studeras. Analyserna baserade på en kraftbalans visar att pluggen vid radiell strömning av en Bingham vätska är oberoende av inträngningslängden. Bingham vätskans inträngning och flöde som funktion av injekteringstiden visas med användning av det konstanta pluggflödet. Skillnader i de två analytiska lösningarna och utveckling av flödet som funktion av tid illustreras. Förklaringen till pluggflödet och utvärderingen av skillnaderna i lösningarna som presenteras förbättrar vår kunskap och förenklar modellering och design av injektering i berg.

I praktiken utförs injektering med icke-Newtonska vätskor i råa sprickor, vilket dock sällan studeras. För att undersöka inverkan av en rå sprickyta vid injektering, presenteras numeriska beräkningar av icke-Newtonian strömning i enskilda råa sprickor, med hjälp av en regulariserad metod. De råa sprickmodellerna är skapade från en laserskannad yta av ett granitbergprov, för att representera realistiska egenskaper hos naturliga bergssprickor. De numeriska resultaten visar icke-linjära beteenden för flödet i råa sprickor orsakade av icke-Newtonska reologiska egenskaper förstärkta av sprickornas råhet. Råheten reducerar avsevärt den effektiva transmissiviteten när Reynolds tal (Re) är relativt stort, dvs Re> 10.

En matematisk modell baserad på Reynolds flödesekvation för inträngning av cementbruk i en slät, vattenmättad, bergspricka presenteras. Modellen är baserad på ett tvåfasflöde, dvs injektering som en Bingham-vätska och grundvatten som en Newtonsk vätska, vilka används för att undersöka påverkan av vattenfasen vid injektering. Modelleringsresultaten för tvåfasflödet visar i allmänhet på vikten av vattenfaten som väsentligen påverkar tryckfördelningen i sprickan, speciellt under härdning av bruket. Sådana effekter beror på viskositetsförhållandet mellan injekterings. Bruket och grundvattnet, vilka blir allt viktigare för fall en med mindre värden på viskositetsskillnaden. Att tillämpa en analytisk lösning baserad på ett enfasflöde, dvs att försumma påverkan av grundvatten vid modellering av ett injekteringförlopp, kommer att överskatta inträngningslängden.

Modellen för tvåfasflöde i enskilda sprickor utvidgas för att simulera icke-Newtonsk strömning i vattenmättade sprick nätverk. Modellen verifieras genom att jämföra simuleringsresultat för utbredningen i spricknät verk med referensdata från Håkansson (1987). Med användning av denna utökade modell undersöktes effekterna på utbredningen av nätverksstruktur och hydraulisk variabilitet, dvs nätgeometri och

fördelning av sprickköppningar, samt reologiska egenskaper, d.v.s. flytgräns och viskositet. Injekteringens utbredning i slumpmässigt genererat tvådimensionellt diskret spricknätverk (2D DFN) simuleras med olika fall av variabilitet i sprickköppning, d.v.s. konstant öppning, baserat på och längdkorrelerad heterogena öppningar, efter en trunkerad lognormal fördelning. Resultaten indikerar att både nätverksstruktur och hydraulisk variation har en stor påverkan för utbredningen i ett 2D DFN-system. Den slumpade nätverksstrukturen och de okorrigerade heterogena öppningarna minskar avsevärt utbredningshastigheten och ökar till stor del variationen i injekterad volym. För längdkorrelerade heterogena öppningar, ökar utbredningshastigheten, medan variabiliteten och förändringen av injekterad volym minskar. De reologiska egenskaperna hos cementbruk, d.v.s. flytgräns och viskositet, påverkar väsentligen utbredningen i ett spricknätverk. Utbredningshastigheten i spricknätverken minskar med en ökning av flyt gräns och viskositet hos cementbruket. Resultaten som presenteras i denna rapport kommer att vara till hjälp vid utformningen och förutsägelsen av bergsprutning.

Nyckelord: berginjektering, Bingham vätska, spricknätverk, tvåfasflöde

CONTENTS

1. INTRODUCTION

1.1 Motivation

Cement grouting is widely used in rock engineering practices to seal rock fractures and limit groundwater inflow. Modeling and analysis of the grout flow is important in design, execution and monitoring of grouting in fractured rocks (Wallner 1976; Lombardi 1985; Hässler, 1991; Håkansson 1993; Warner 2004; Gustafson and Claesson, 2005; Funehag and Fransson 2006; U.S. Army Corps of Engineers, 2014; Stille 2015; Li et al, 2016; Liang 2019; Zou et al. 2018; 2019; 2020). Modeling of grouting in rock fractures is important for effective design and performance of grouting activities in ever-increasing demands of underground rock engineering projects (Stille 2015).

The cement grouts mostly used in practice are typically non-Newtonian fluids (Håkansson 1993; Nguyen et al., 2006; Rahman et al. 2015; Shamu and Håkansson 2019). In particular, the Bingham model has been frequently applied to model grouts behavior, due to its simplicity and physically based parameters (Hässler, 1991; Håkansson 1993; Rahman et al. 2015; Zou et al. 2018; 2019).

Cement grouts are typically injected through boreholes with a constant pressure (Wallner 1976; Hässler 1991; Stille 2015). Two types of flow configurations are often used to model cement grout flow in fractured rock: radial flow and channelized flow between parallel plates (Hässler 1991). Figure 1 illustrates the relevance of both flow configurations when considering multiple fractures. Approximately radial flow may occur in the fracture intersecting the injection borehole, while channelized flow can take place through connecting fractures (Figure 1).

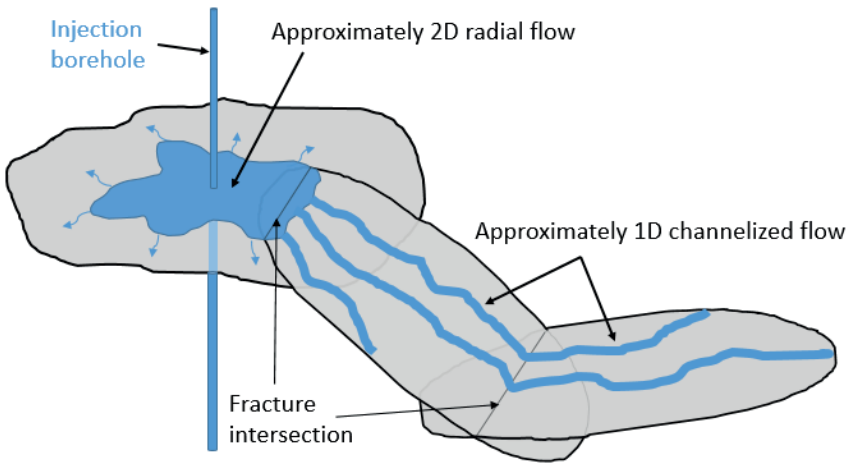

Figure 1. Schematic diagram of the radial (2D) and channel (1D) representation of cement grout flow in multiple rock fractures.

At present, simulation of the rock grouting process remains a challenge, since the rock grouting process involves complex fluids propagation in rock fractures with complex geometrical structures. In practice, design of rock grouting relies heavily on analytical solutions based on simplified rheological models for grouts and idealized geometrical conditions for single rock fractures. In order to derive analytical solutions for the Bingham type of grout propagating in single fractures, from an intersecting borehole, the process is generally idealized as two-dimensional (2D) radial flow between parallel planar disks (e.g., Wallner 1976; Lombardi 1985; Hässler 1991, Sui et al., 2015; Stille 2015; Zhang 2018). Dai and Bird (1981) derived a solution for flowrate by adapting the solution of one-dimensional (1D) plane channel flow. By using the flowrate equation presented in Dai and Bird (1981), Gustafson and Claesson (2005) derived a solution for the relative penetration length of grout as a function of time, which lay the theoretical basis of the real time grouting control (RTGC) method for grouting design (Kobayashi et al. 2008; Stille et al., 2009). In this solution, the plug flow region in the radial flow of a Bingham fluid is an increasing function of the radial distance.

This solution has been extended and widely used in grouting study and practice (e.g., Fransson et al. 2007; Kobayashi et al. 2008; Stille et al. 2012; Funehag and Thörn 2014, 2018; Rafi and Stille 2014, 2015; Stille 2015). The validity of the solution by Gustafson and Claesson (2005) was questioned by El Tani (2009; 2012; 2013). El Tani (2012) derived a solution for radial flow of a Bingham fluid and the relative grout penetration with time; he determined the plug flow region by using the energy dissipation equation. The results of El Tani (2012) show that the plug flow region is independent of fracture radius at each time step and the relative size of the plug flow region (i.e., ratio between the height of the plug flow region and the fracture aperture) equals the relative penetration length (i.e., ratio between the penetration length and the maximum penetration length) when the grout is propagating, which is the same as for 1D channel flow.

The diverging perceptions of the plug flow region directly led to the two alternative solutions for the grout penetration (Gustafson and Claesson 2005; El Tani 2012; Gustafson et al 2013). Rafi and Stille (2015) compared the two solutions with results of the relative penetration length only for the range of relative time t_D smaller than 0.6. t_D is a dimensionless time defined as $t_D = \frac{t{\tau_0}^2}{6\mu(P_g - P_w)}$ in Gustafson and Claesson (2005), where t is the injection time, τ_0 is the yield stress, μ is the plastic viscosity, P_g is the injection pressure and P_w is the in situ groundwater pressure. It is found that at the range of relative time smaller than 0.2, the two results are almost the same. Comprehensive verifications of the two solutions have not been done to date, and the issue of the shape of plug flow region has not been fully resolved.

In most underground projects, the fractured rocks are saturated with groundwater and therefore, the grouts spreading in rock fractures is actually a two-phase flow process where the groundwater is replaced by the penetrating grouts (Hässler 1991). At present, most analytical solutions (e.g., Gustafson and Claesson 2005; El Tani 2012; Gustafson et

al 2013) are based on the assumption that the flow of groundwater is negligible. At the early stage, Hässler (1991) developed a numerical model to calculate the flow velocity in a structured network of planar fractures filled with both water and a Bingham fluid (grout), but without a comprehensive examination of the influence of the water flow. It is therefore of interest to systematically elucidate the impact of water flow but also to provide a more general two-phase formulation of grout flow that can be used for further studies of alternative boundary conditions (e.g., with variable injection pressure) relevant for execution of grouting works.

In reality, rock fracture surfaces are rough and fracture apertures are spatially variable, which causes important uncertainty for modeling of fluid flow and solute transport in fractured rocks (e.g., Zou et al. 2016; 2017). For groundwater (Newtonian fluid), many experimental and numerical studies have revealed that the rock fracture surface roughness significantly reduces the effective transmissivity of rock fractures. The hydraulic aperture is therefore smaller than the mechanical aperture (Zou et al. 2015; 2017). However, for non-Newtonian fluids, e.g., cement grouts and drilling muds, such impact of fracture surface roughness have not been investigated. Therefore, the consequence of assuming the fracture is homogeneous with a constant aperture, as adopted by many theoretical studies, has not been studied in previous works.

Rock masses contain complex fracture networks, which provide dominant pathways for groundwater flow and mass transport (Long et al 1982). The discrete fracture network (DFN) model has been widely applied to simulate groundwater flow and solute transport in fractured rocks both in 2D (Cacas et al., 1990; Baghbanan and Jing 2007; Dershowitz et al., 2007; Zhao et al, 2014) and 3D (Cvetkovic and Frampton 2012; Dreuzy et al., 2012; Frampton et al., 2019). To date, only a few studies have simulated non-Newtonian grout propagation in fracture networks, e.g., Mohajerani et al., (2017) modeled Bingham grout propagation in 2D discrete fracture networks without consideration of the groundwater flow. By considering groundwater flow, Hässler (1991), and Erisson et al., (2000) simulated Bingham grout flow in 2D structured fracture networks using an implicit numerical model. Fidelibus and Lenti (2012) developed a numerical pipe network model and modeled Bingham grout propagation in 2D structured networks. Deng et al., (2018) simulated Bingham grout penetration in 3D fracture networks using a computational fluid dynamics (CFD) approach. In general, these studies only considered grouts as Bingham fluids. Most previous studies have not been validated, except that Hässler (1991), Erisson et al., (2000), and Mohajerani et al., (2017) compared their simulation results with the experimental data by Håkansson (1987). Moreover, most previous studies only illustrated grout flow in regular channels or pipe networks with simple geometries without considering important geological features of rock fracture networks, except Mohajerani et al., (2017) and Deng et al., (2018), and also without considering impacts of rheological properties and natural hydraulic variability. It is known that the fracture network structure and hydraulic aperture variability has important effects on the groundwater flow and solute transport processes in fractured rocks (e.g., Long et al 1982; Cacas et al., 1990; Baghbanan and Jing 2007; Dershowitz et al., 2007; Cvetkovic and Frampton 2012;

Dreuzy et al., 2012; Frampton et al., 2019). However, the impacts of network structure and hydraulic variability as well as rheological properties on cement grout propagation in water-saturated fracture networks remain open issues.

1.2 Objectives

The general objective of this project is to improve predictions, design, and execution of rock grouting, by introducing numerical simulations and possibly new rheological models for cement-based grouts. We attempt to fill aforementioned knowledge gaps by modeling cement grouts propagation in a single fracture and 2D fracture networks, by considering the presence of water flow and fracture network structures with variable hydraulic apertures. Our focuses are on the impact of **i)** complex geometrical conditions (i.e., surface roughness, fracture network structures and aperture variability) and **ii)** complex non-Newtonian rheological properties (i.e., yield stress and time-dependent viscosity) on grout propagation in rock fractures. Our specific objectives are:

(1) Clarify the confusion existing in the two solutions regarding the shape of the plug flow region in 2D radial flow of a Bingham fluid for application of the RTGC method.

(2) Evaluate the discrepancy in the two solutions based on the two alternative shapes of the plug flow region in 2D radial flow of a Bingham fluid for theoretical analyses of grout propagation in rock fractures.

(3) Present the grout volume and flowrate as functions of grouting time and relative penetration length using the radius-independent plug flow region.

(4) Investigate the impact of surface roughness on non-Newtonian cement grout flow in rock fractures by numerical simulations of Bingham grout flow in a single rough-walled fracture.

(5) Present a two-phase flow model of non-Newtonian cement grout propagation combined with a Reynolds type of equation.

(6) Investigate the potential impact of water flow on grout propagation for different viscosity ranges.

(7) Illustrate the combined effect of the water phase and grout hardening process for different parameter ranges.

(8) Extend the two-phase flow model based on a single fracture for simulating cement grouts (Bingham fluids) propagation in water saturated fracture networks.

(9) Verify the two-phase fracture network model using the benchmark experimental data by Håkansson (1987).

(10) Illustrate and quantify the two-phase propagation processes of cement grouts in saturated fracture networks.

(11) Investigate the impact of fracture network structure and hydraulic variability on cement grout propagation by statistical analyses of multiple realizations.

(12) Investigate the impact of rheological properties on the propagation process in saturated fracture networks.

1.3 Publications from this project

The results of this project have been published or presented in international journals or conferences, including:

(1) Zou L, Håkansson U, Cvetkovic V. Cement grout propagation in two-dimensional fracture networks: Impact of structure and hydraulic variability. International Journal of Rock Mechanics and Mining Sciences. Volume 115, March 2019, Pages 1-10. https://doi.org/10.1016/j.ijrmms.2019.01.004

(2) Zou L, Håkansson U, Cvetkovic V. Two-phase cement grout propagation in homogeneous water-saturated rock fractures. International Journal of Rock Mechanics and Mining Sciences. Volume 106, June 2018, Pages 243–249. https://doi.org/10.1016/j.ijrmms.2018.04.017.

(3) Zou L, Håkansson U, Cvetkovic V, Analysis of Bingham fluid radial flow in smooth fractures, Journal of Rock Mechanics and Geotechnical Engineering, Volume 12, Issue 5, October 2020, Pages 1112-1118. https://doi.org/10.1016/j.jrmge.2019.12.021

(4) Zou L, Håkansson U, Cvetkovic V, Reply to Discussion on 'Analysis of Bingham fluid radial flow in smooth fractures', Journal of Rock Mechanics and Geotechnical Engineering, in press. https://doi.org/10.1016/j.jrmge.2021.04.001

(5) Zou L, Håkansson U, Cvetkovic V, Yield-power-law fluid propagation in water-saturated fracture networks with application to rock grouting, Tunnelling and Underground Space Technology, Volume 95, 2020, 103170. https://doi.org/10.1016/j.tust.2019.103170

(6) Zou L, Håkansson U, Cvetkovic V, Radial propagation of yield-power-law fluids into water-saturated homogeneous fractures with application to rock grouting, Volume 130, June 2020, 104308. https://doi.org/10.1016/j.ijrmms.2020.104308.

(7) Zou L, Håkansson U, Cvetkovic V, Characterization of effective transmissivity for cement grout flow in rock fractures, the 9th Nordic Grouting Symposium, September 2-3, 2019, Helsinki, Finland.

(8) Zou L, Håkansson U, Cvetkovic V, Cement grout propagation in 2D fracture networks: impact of rheology, the 14th ISRM congress, September 13-18, 2019, Foz do Iguaçu, Brazil.

(9) Zou L, Håkansson U, Cvetkovic V, Non-Newtonian grout flow in single rough-walled rock fractures, Bergdagarna 2019. March 19, 2019, Stockholm.

(10) Zou L, Håkansson U, Cvetkovic V, Impacts of Elastic Jacking on Rock Grouting, In Proceeding of the 10th Asian Rock Mechanics Symposium, 29 October to 03 November 2018, Singapore.

(11) Zou L, Håkansson U, Cvetkovic V. Modeling of rock grouting in saturated variable aperture fractures. Bergdagarna 2018. March 20, 2018, Stockholm.

(12) Zou L, Håkansson U, Cvetkovic V. Non-Newtonian fluid flow in 2D fracture networks. AGU Fall Meeting 2017. 11-15 Dec. 2017, New Orleans.

2. SINGLE-PHASE BINGHAM GROUT RADIAL FLOW IN HOMOGENEOUS FRACTURES

As mentioned in Section 1.1, there were two solutions for single-phase Bingham grout radial flow in homogeneous fractures in the literature that has caused confusion in the rock grouting research community. In this Chapter, we present our analyses of single-phase Bingham grout radial flow in homogeneous fractures based on the assumption that the vertical velocity across the aperture is negligible. More details can be found in Zou et al. (2020) and Hoang et al. (2020). More details of the other solution with considering the vertical velocity can be found in Dai and Bird (1981) and Gustafson et al. (2013). More detailed discussions of the two solutions can be found in Hoang et al. (2020) and Zou et al. (2021).

2.1 Physical considerations and assumptions

Figure 1 presents the physical system of grouting in 2D radial flow for an idealized planar fracture represented by a pair of parallel disks. The fracture hydraulic aperture is 2B (it is often characterized by hydraulic test in applications). The cement grout; considered behaving as a Bingham fluid; is injected through a perpendicular borehole with a constant effective grout pressure P_g. The radius of the injection borehole is r_0. The pressure gradient between the grout pressure and the in-situ groundwater pressure P_w propagate the grout from the borehole into the fracture. Cross-section A-A shows the grout propagating in the fracture. The distance between the borehole and the grout front represents the penetration length $I(t)$, which is a function of the grouting time.

It is assumed that the viscosity of the cement grout (approximately 0.01-0.015 $Pa \cdot s$) is higher than the viscosity of groundwater (normally around 0.001 $Pa \cdot s$) and that the pressure drop for the groundwater flow is negligible (i.e., the pressure of groundwater is constant). Therefore, at each snapshot in time of the grouting process, the flow of grout can be simplified as steady-state radial flow. In our analysis, it is also assumed that the grout is incompressible, inertial effects are negligible and that the pressure gradient and vertical velocity across the aperture is negligible in our analysis since the fracture aperture is much smaller than its lateral dimensions.

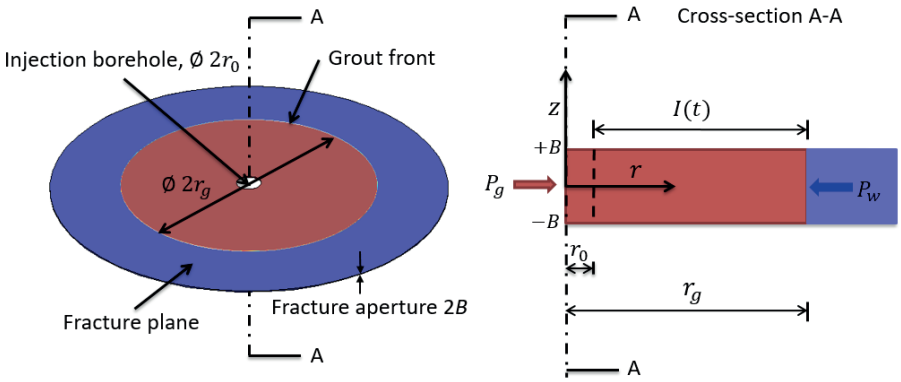

Figure 2 Schematic of grouting with 2D radial flow.

2.2 Mathematical model for radial flow of single-phase Bingham fluid

Given the above assumptions, mass and momentum conservation leads to the following governing equations for 2D radial flow:

$$\frac{\partial}{\partial r}(r\, v_r) = 0 \tag{1}$$

$$\frac{\partial P}{\partial r} + \frac{\partial \tau_{zr}}{\partial z} = 0 \tag{2}$$

where v_r is the radial velocity, P is the pressure and τ_{zr} is the shear stress. For a Bingham fluid, the shear stress τ_{zr} is expressed as

$$\begin{cases} \tau_{zr} = \tau_0 + \mu \frac{\partial v_r}{\partial z} & \left|\frac{\partial v_r}{\partial z}\right| > 0 \\ \tau_{zr} < \tau_0 & \frac{\partial v_r}{\partial z} = 0 \end{cases} \tag{3}$$

where τ_0 is the yield stress. The boundary conditions for this system are

$$P(r = r_0) = P_g, P\left(r = r_g\right) = P_w \tag{4}$$

$$v_r(r, z = \pm B) = 0 \tag{5}$$

$$\frac{\partial v_r}{\partial z}\left(r, z = \pm z_p\right) = 0 \tag{6}$$

Equation (4) represents the known pressure boundary conditions; equation (5) denotes the no-slip boundary condition at the fracture walls, and equation (6) represents the zero-shear rate condition in the plug flow region.

2.3 Analytical solution for radial flow of single-phase Bingham fluid

Equation (1) implies that rv_r is a function independent of r, but dependent on the radial angle θ and the vertical coordinate z, i.e., $rv_r = f(\theta, z)$. In addition, the solution of radial velocity v_r is expected to be symmetrical with respect to the z-axis, i.e., the solution is independent on θ. Therefore, the radial velocity v_r can be expressed as

$$r\,v_r = f(z),\ v_r = \frac{f(z)}{r} \tag{7}$$

By invoking equations (3) and (7) into equation (2), we get

$$-r\frac{\partial P}{\partial r} = \mu\frac{\partial^2 f(z)}{\partial z^2} = a_0 \tag{8}$$

where a_0 is an integration constant. By integrating both sides of equation (8) separately, we obtain

$$P = -a_0\ln(r) + a_1 = \frac{P_w - P_g}{\ln\left(\frac{r_g}{r_0}\right)}\ln(r) + P_g - \frac{P_w - P_g}{\ln\left(\frac{r_g}{r_0}\right)}\ln(r_0) \tag{9}$$

$$\frac{\partial P}{\partial r} = -\frac{a_0}{r} = \frac{P_w - P_g}{\ln\left(\frac{r_g}{r_0}\right)}\frac{1}{r} \tag{10}$$

$$\frac{\partial f(z)}{\partial z} = \frac{a_0}{\mu}z + a_2 = \frac{P_g - P_w}{\ln\left(\frac{r_g}{r_0}\right)}\frac{1}{\mu}(z - z_p) \tag{11}$$

$$f(z) = \frac{a_0}{2\mu}z^2 + a_2 z + a_3 = \frac{1}{2\mu}\frac{P_g - P_w}{\ln\left(\frac{r_g}{r_0}\right)}(z^2 - B^2) - \frac{z_p}{\mu}\frac{P_g - P_w}{\ln\left(\frac{r_g}{r_0}\right)}(z - B) \tag{12}$$

where a_1, a_2 and a_3 are integration constants that can be determined by introducing the boundary conditions, i.e., equations (4-6), written as $a_0 = \frac{P_g - P_w}{\ln\left(\frac{r_g}{r_0}\right)}$, $a_1 = P_g + a_0\ln(r_0)$, $a_2 = -\frac{a_0}{\mu}z_p$ and $a_3 = -\left(\frac{a_0}{2\mu}B^2 - \frac{a_0 z_p}{\mu}B\right)$, and z_p is half of the plug flow region. It is worth mentioning that in the solution by Gustafson and Claesson (2005) and Gustafson et al. (2013) they did not use the mass balance equation to determine the pressure as in equation (9). Instead, they deduced a complicated solution by solving the implicit differential equation for the pressure.

The solution of the velocity, v_r, is an even function of z. For the upper half aperture, $0 < z \le B$, the velocity can be expressed as

$$v_r(z_p \le z \le B) = \frac{1}{2\mu}\left(-\frac{\partial P}{\partial r}\right)(z^2 - B^2) - \frac{z_p}{\mu}\left(-\frac{\partial P}{\partial r}\right)(z - B) \tag{13}$$

$$v_r(0 \le z < z_p) = \frac{1}{2\mu}\left(-\frac{\partial P}{\partial r}\right)\left({z_p}^2 - B^2\right) - \frac{z_p}{\mu}\left(-\frac{\partial P}{\partial r}\right)\left(z_p - B\right) \tag{14}$$

By integration of the velocity across the aperture, the flowrate Q is obtained as

$$Q = 2\int_0^B 2\pi r\, v_r\, dz = -\frac{2\pi r\, B^3}{3\mu}\frac{\partial P}{\partial r}\left(2 - 3\frac{z_p}{B} + \frac{{z_p}^3}{B^3}\right) = \frac{2\pi\, B^3}{3\mu}\frac{(P_g - P_w)}{\ln\left(\frac{r_g}{r_0}\right)}\left(1 - \frac{z_p}{B}\right)^2\left(2 + \frac{z_p}{B}\right) \quad (15)$$

Since $\frac{\partial \mathrm{P}}{\partial \mathrm{z}} = 0$ is assumed, the pressure is a function of r only (see equation 10). The momentum equation (2) is integrated over z to obtain

$$\tau_{zr} = \left(-\frac{\partial P}{\partial r}\right) z + C \quad (16)$$

where C is an integration constant to be determined by introducing the boundary condition at $z = z_p$ (the interface between the solid and fluid regions), i.e., equation (6), as $C = \tau_0 + \frac{\partial P}{\partial r} z_p$. For the fluid part, the shear stress is

$$\tau_{zr} = \tau_0 + \left(-\frac{\partial P}{\partial r}\right)(z - z_p) \quad (17)$$

For the solid (plug) region (i.e., $0 \le z < z_p$), the shear rate is 0, and the shear stress is explicitly given by the definition of Bingham model, i.e., $\tau_{zr} < \tau_0$. It implies that the shear stress can be any value below the yield stress in the plug flow region.

Determining the plug flow region is an important step to obtain the complete analytical solution for radial flow of Bingham fluids. The simplest and most straightforward way to determine the plug flow region is by using a force balance. Specifically, the difference between the force at the injection borehole and at the grout penetration front is equal to the total friction force on the wall surfaces. This can be expressed as

$$2\int_{r_0}^{r_g} \tau_w\, dr = 2B(P_g - P_w) \quad (18)$$

where the shear stress on the wall τ_w is

$$\tau_w = \tau_0 + \left(-\frac{\partial P}{\partial r}\right)(B - z_p) \quad (19)$$

The integration of shear stress on the wall gives $\tau_0(r_g - r_0) + (P_g - P_w)(B - z_p)$. Half of the plug flow region z_p can then be obtained as

$$z_p = \frac{\tau_0(r_g - r_0)}{P_g - P_w} \quad (20)$$

which implies that the plug flow region is independent of the radius r, i.e., it is constant along the radial distance. Since the shear stress and pressure are independent of the circumferential angle, we can take the radial cross-section A-A (see Figure 1) to illustrate the force balance in Figure 3. Note that the same radius-independent plug flow region can also be determined by using the energy dissipation equation (El Tani, 2012).

Quantifying the shear stress is a key step that has led to different plug flow regions, following from different ways of determining the integration constant C in equation (16). It is common to assume that C=0, i.e., $\tau_{zr} = 0$ for $z = 0$; such a condition however is

applicable only for fluids without yield stress, e.g., Newtonian and power-law fluids. Dai and Bird (1981) essentially adapted this assumption from the solution of 1D slit flow by a similarity or analogy argument. For Bingham fluid flow in a 1D channel, half of the plug flow region is

$$z_p = \tau_0 \left|\frac{\Delta P}{L}\right|^{-1} \tag{21}$$

where ΔP and L are the pressure difference and distance between the injection inlet and the fracture length, respectively (Bird et al. 1960). In the solution for 2D radial flow by Dai and Bird (1981), half of the plug flow region is obtained by replacing $\frac{\Delta P}{L}$ with $\frac{dP}{dr}$ in equation (21). The plug flow region then becomes a function of the radius r, since $\frac{dP}{dr}$ is a nonlinear function of the radius, according to equation (10). This yields a different result for the flowrate or grouting penetration from the case when C≠0 in equation (16). A schematic illustration of radius-independent and radius-dependent plug flow regions for radial 2D flow is shown in Figure 3.

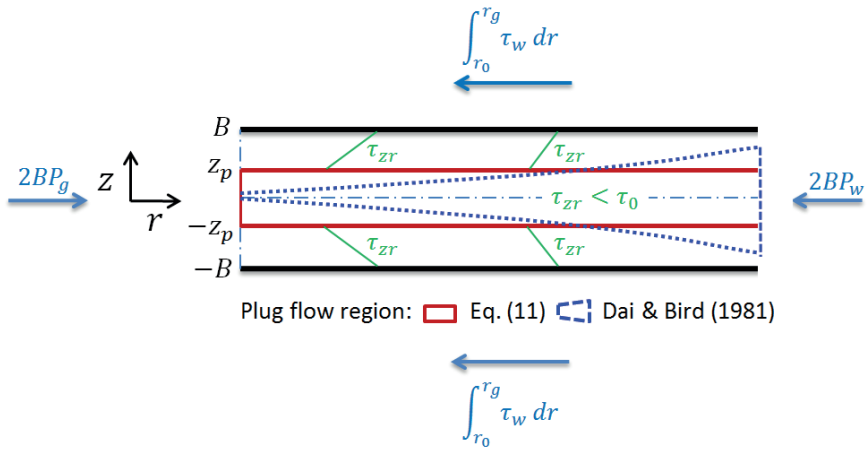

Figure 3 demonstration of shear stress, plug flow region and force balance in a cross-section for radial flow of Bingham fluids.

2.4 Quasi-steady solution: theory for the RTGC method

The grout penetration length is connected with the mean velocity of the grout front $\bar{v}_r$, written as (Gustafson and Claesson, 2005)

$$\bar{v}_r = \frac{Q}{A} = \frac{dI}{dt} \tag{22}$$

where A denotes the surface area of the grout front (i.e., $A = 4B\pi r_g$) and I denotes the penetration length (i.e., $I = r_g - r_0$). Note that the maximum penetration length will be

reached when the plug flow region equals to the aperture, i.e., $z_p = B$. Hence, the maximum penetration length I_{max} can be obtained as

$$I_{max} = \frac{B(P_g - P_w)}{\tau_0} \tag{23}$$

The relative penetration length is defined as

$$I_D = \frac{I}{I_{max}} = \frac{\tau_0(r_g - r_0)}{B(P_g - P_w)} \tag{24}$$

Inserting the constant plug flow region, i.e., equation (20) into equation (24) yields

$$I_D = \frac{z_p}{B} \tag{25}$$

It reveals that the relative penetration length equals to the relative width of the plug flow region (i.e., the ratio of plug flow region to the aperture) for 2D radial flow, which is the same as for 1D channel flow.

Substituting equations (15) and (24) into equation (22) yields

$$\frac{dI_D}{dt} = \frac{{\tau_0}^2}{6\mu(P_g - P_w)} \cdot \frac{1}{I_D} \cdot \frac{I_D B(P_g - P_w)/\tau_0}{I_D B(P_g - P_w)/\tau_0 + r_0} \cdot \frac{(2 - 3\, I_D + {I_D}^3)}{\ln\,(I_D B(P_g - P_w)/\tau_0 r_0 + 1)} \tag{26}$$

For simplicity, a dimensionless time $t_D = t/t_0 = \frac{t{\tau_0}^2}{6\mu(P_g - P_w)}$ and parameter $\gamma = \frac{I_{max}}{r_0} = \frac{B(P_g - P_w)}{r_0 \tau_0}$ were introduced by Gustafson and Claesson (2005), to obtain the relative penetration function. Equation (26) can then be rewritten as

$$\frac{dI_D}{dt_D} = \frac{(2 - 3\, I_D + {I_D}^3)}{(I_D + 1/\gamma)\ln\,(I_D\gamma + 1)}, \quad \frac{dt_D}{dI_D} = \frac{(I_D + 1/\gamma)\ln\,(I_D\gamma + 1)}{(2 - 3\, I_D + {I_D}^3)} \tag{27}$$

The closed-form solution of grouting time with the relative penetration length can be obtained by integration of equation (27), which was presented in El Tani (2012). The exact formula for the closed-form solution is complicated and contains series approximation. In practice, equation (27) can be easily solved by numerical integration methods. Note that using the radius-dependent plug flow region and considering the vertical velocity across the aperture, Gustafson and Claesson (2005) obtained a different and more complicated solution for the relative penetration function.

In addition to the grout penetration length, the injected grout volume and flowrate as functions of grouting time are of great importance in grouting design and practice, since they are often taken as stop criteria for grouting (Gustafson and Claesson, 2005; Gustafson and Stille 2005; Kobayashi et al. 2008; Rafi and Stille 2014; Stille 2015). The injected grout volume V_g can be obtained through the grout penetration length I, written as (Gustafson and Claesson, 2005)

$$V_g = 2\pi B[(r_0 + I)^2 - {r_0}^2] = 2\pi B I^2(1 + 2r_0/I) \tag{28}$$

The maximum injection volume $V_{g,max}$ arrives when $I = I_{max}$, which is

$$V_{g,max} = 2\pi B {I_{max}}^2 (1 + 2/\gamma) \tag{29}$$

where $\gamma = I_{max}/r_0$. Then the relative volume of injected grout is

$$V_D = \frac{V_g}{V_{g,max}} = {I_D}^2 \cdot \frac{1+2/\gamma I_D}{1+2/\gamma} \tag{30}$$

where is the relative penetration length, $I_D = I/I_{max}$. Using our proposed formula of relative penetration rate, i.e., equation (27), the evolution of grouting flowrate Q_g can be determined according to its definition, written as

$$Q_g = \frac{dV_g}{dt} = \frac{dV_D}{dt_D} \cdot \frac{V_{g,max}}{t_0} = \frac{2I_D+2/\gamma}{1+2/\gamma} \cdot \frac{dI_D}{dt_D} \cdot \frac{V_{g,max}}{t_0} = \frac{2I_D+2/\gamma}{1+2/\gamma} \cdot \frac{(2-3\,I_D+{I_D}^3)}{(I_D+1/\gamma)\ln(I_D\gamma+1)} \cdot \frac{V_{g,max}}{t_0} \tag{31}$$

A simplified empirical formula of relative penetration as function of dimensionless grouting time was proposed by Gustafson and Stille (2005) to approximate the evolution of flowrate, due to the complexity of the original solution of grout penetration that was developed in Gustafson and Claesson (2005) and Gustafson et al (2013). However, by using the solution with radius-independent plug flow region and without considering the vertical velocity, a closed-form solution of flowrate as function of grouting time can explicitly be obtained for the first time without any approximation; the result is shown in equation (31). This closed-form solution of the flowrate can be directly applied for control and monitoring in grouting practice.

2.5 Illustration examples: comparison of the two solutions

The results of penetration length and flowrate from the two solutions are compared within the full range of relative penetration length, shown in Figures 4 and 5. According to the theoretical analysis, the steering parameter in the functions of relative penetration length, injected grout volume and flowrate is γ. The relative penetration and the flowrate evolution curves for different γ values are calculated and compared in Figures 4 and 5. The adopted parameters (typically used in grouting practice) for the calculation of flowrate are summarized in Table 1.

Table 1. Grouting parameters for the illustration example

Parameters	Units	Values
Aperture, 2B	[μm]	100
Borehole radius, $\boldsymbol{r_0}$	[m]	0.025
Viscosity of grout, $\boldsymbol{\mu}$	[Pa·s]	0.025
Yield stress of grout, $\boldsymbol{\tau_0}$	[Pa]	5
Grouting pressure, $\boldsymbol{P_g - P_w}$	[MPa]	0.025, 0.25, 0.75 and 2.5

Steering parameter, $\boldsymbol{\gamma}$	[-]	10, 100, 300 and 1000
Characteristic time, $\boldsymbol{t_0}$	[min]	2.5, 25, 75 and 250
Maximal penetration, $\boldsymbol{I_{max}}$	[m]	0.25, 2.5, 7.5 and 25
Maximal injection volume, $\boldsymbol{V_{g,max}}$	[L]	0.024, 2.00, 17.79 and 196.74

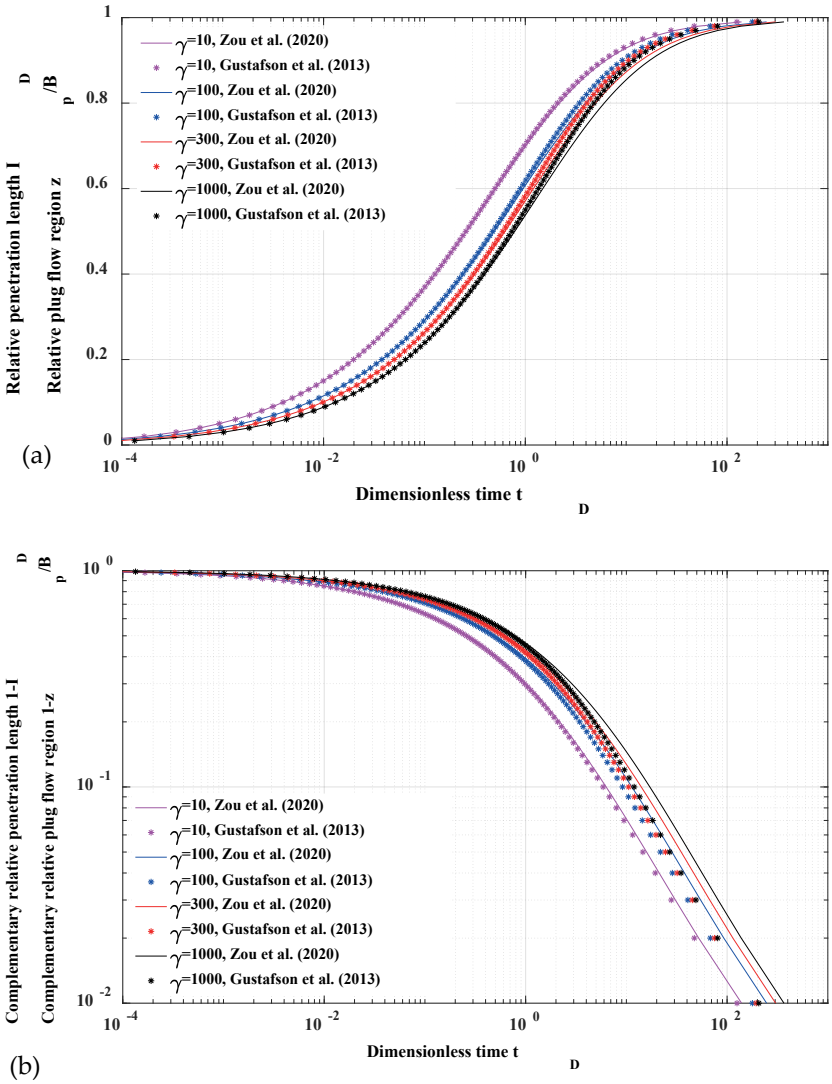

Figure 4 Comparison between and the two approximate analytical solutions of the relative penetration length with dimensionless grouting time (a) and (b) log-log plot of the complementary relative penetration length (1- I_D), highlighting the discrepancy in relatively longer grouting time (i.e., $t_D > 1$).

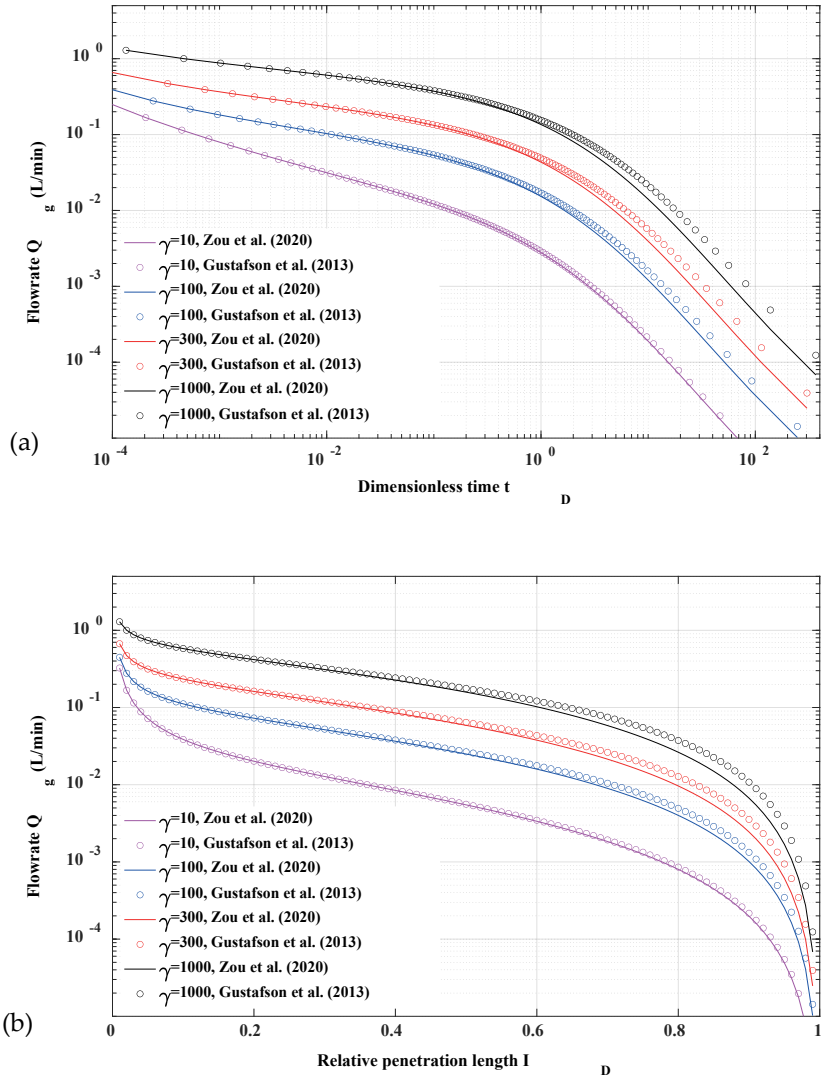

Figure 5 Comparison between and the two approximate analytical solutions of the grout flowrate evolution with (a) dimensionless grouting time and (b) relative penetration length.

As shown in Figure 4a, the grout penetration is increasing but decelerating with time, regardless of the parameter γ. In contrast, the grout flowrate is decreasing with grouting

time (Figure 5a) as well as the relative penetration length (Figure 5b). With the increase of γ, the penetration becomes relatively slower, and the corresponding flowrate becomes relatively larger. By using the penetration and flowrate functions, the grouting process can be fully defined for design, monitoring and quality assurance in grouting applications.

In general, the results of the two approximate solutions are in good agreement, especially within a shorter penetration distance (i.e., $I_D < 0.5$) and a lower dimensionless time (i.e., $t_D < 1$). With the increases of penetration distance and grouting time, the two solutions gradually deviate in a small range. A log-log plot of the complementary relative penetration length (1- I_D) is presented in Figure 4b, to highlight the discrepancy in the relatively longer grouting time (i.e., $t_D > 1$). Such deviations demonstrated that the two solutions are not exactly identical, but the differences in results of penetration distance and flowrate between the two solutions are negligible.

2.6 Discussion on the two solutions

Recently, Hoang et al. (2021) discussed our paper Zou et al. (2020). In our paper, we made a statement that Dai and Bird's solution for 2D radial Bingham fluid flow between parallel plates violates mass balance. Hoang et al. (2020) pointed out that Dai and Bird's solution does not violate the mass balance because Dai and Bird's solution and our analysis are based on different assumptions, i.e., with consideration of the vertical velocity component in the continuity equation or not, which leads to two different approximation models. This discussion helps to thoroughly clarify the existing confusion in the two solutions for analyzing rock grouting. Specifically, the confusion regarding Dai and Bird's solution and its application to rock grouting has been raised because no explicit mathematical models, i.e., the governing equations, were presented either in Dai and Bird (1981) nor in the following rock grouting literature, e.g., Gustafson et al. (2013). In the discussion by Hoang et al. (2021), the governing equations of the two approximation models with associated solutions were clearly summarized in their Equations 5, 6 and 7, indicating that the two models are based on different assumptions, i.e., with or without considering the vertical velocity.

Note that the shape of the plug flow region varies in the two different approximation models. Specifically, the plug flow region in the model presented in Zou et al. (2020) is independent of the radius; whereas in the model (Equations 5, 6 and 7) presented in Hoang et al. (2021), the plug flow region increases with the radius. In higher orders of approximation models, the plug flow region can be more complex (e.g., Muravleva 2017). The reason for the obtained different shapes of plug flow region in the two approximation models is indicated in the discussion by Hoang et al. (2021), which is due to the application of different boundary conditions for the shear stress. Specifically, we use the boundary condition on the surface of the plug flow region, while the other model sets shear stress equal to zero in the middle of the fracture aperture in the plug flow region. We think that the shear stress in the plug region is undefined according to the definition of the Bingham model, which only defines that the shear stress is below the yield stress

in the plug flow region (it implies that the shear stress can be any value below the yield stress in the plug flow region), see Equation 3 in Zou et al. (2020) or Equations 1 and 2 in Hoang et al. (2021). Moreover, the Bingham model is an idealized rheological model and its validity for any realistic fluids remains an open question (Barnes 1999). Therefore, the real shape of the plug flow region for realistic fluids/grouts or even the existence of a rigid plug flow region remains unknown at this point.

With the understanding that Dai and Bird's solution and our analysis are two separate approximation models, we should clarify that the two types of analytical solutions for rock grouting, presented in Gustafson et al. (2013) and Zou et al. (2020), respectively, are both approximation solutions, i.e., neither of them is an exact solution. However, as noted in the discussion by Hoang et al. (2021), the solution presented in Zou et al. (2020) is much simpler compared to the one based on Dai and Bird's solution. More importantly, the solution presented in Zou et al., (2020) is more relevant to the boundary condition commonly applied in rock grouting with a controlled injection pressure, where the solution for the pressure is explicit with respect to the boundary pressures (see Equations 9 and 10). In contrast, Dai and Bird's solution is more relevant to the boundary condition of known constant flowrate, where the solution for the pressure needs to be solved from the flowrate equation, i.e., Equation 4 in Hoang et al. (2021). Considering that the difference between solutions from the two models is relatively small (see Figure 6 in Hoang et al., 2021) and that the predicted grout propagation lengths using the two models are very close (see Figures 4 and 5), it is recommended using the simpler solution presented in this report for rock grouting analysis in practice.

3. SINGLE-PHASE BINGHAM GROUT FLOW IN SINGLE ROUGH-WALLED FRACTURES

In this Chapter, we present numerical simulation results of single-phase Bingham grout flow in single rough-walled fractures, aiming to investigate the impact of fracture surface roughness on Bingham grout flow in natural rock fractures. More details can be found in Zou et al (2019).

3.1 Governing equations for Bingham fluids flow

The general governing equations based on mass and momentum conservation for incompressible fluid flow can be written as

$$\nabla \cdot \mathrm{u} = 0 \tag{32}$$

$$\frac{\partial}{\partial \mathrm{t}}(\rho \mathrm{u}) + \rho\, \mathrm{u} \cdot \nabla \mathrm{u} = -\nabla \mathrm{p}\mathrm{I} + \nabla \cdot \tau + \rho \mathrm{g} \tag{33}$$

where $\mathrm{u}\ (\mathrm{m/s})$ is the fluid velocity vector, ρ is fluid density, t is time, P is pressure, I is the identity matrix and g is acceleration of gravity.

The linear Bingham rheology model was widely adopted for theoretical analyses in the past decades, given by

$$\begin{cases} \tau_{\mathrm{ij}} = \left(\frac{\tau_0}{|\dot{\gamma}_{\mathrm{ij}}|} + \mu_{\mathrm{B}}\right) \dot{\gamma}_{\mathrm{ij}}, & |\tau_{\mathrm{ij}}| > \tau_0 \\ \dot{\gamma}_{\mathrm{ij}} = 0 & \text{otherwise} \end{cases} \tag{34}$$

where τ_{ij} is shear stress tensor, $\dot{\gamma}_{ij}$is the shear rate (rate-of-strain) tensor, τ_0 is the yield stress and μ_{B} is the plastic viscosity. The Bingham fluid is an idealized non-Newtonian fluid that may not exist in reality. Papanastasiou (1987) developed a modified Bingham model (referred to as the Bingham-Papanastasiou model) by adding an exponential term to smoothly approximate the yield stress, which is able to represent the more realistic visco-plastic behavior of non-Newtonian fluids, written as

$$\tau_{\mathrm{ij}} = \left\{\mu_{\mathrm{B}} + \frac{\tau_0}{|\dot{\gamma}_{\mathrm{ij}}|}\left[1 - \exp(-\mathrm{m}|\dot{\gamma}_{\mathrm{ij}}|)\right]\right\} \dot{\gamma}_{\mathrm{ij}} \tag{35}$$

where the m is an exponential index. As m is relatively large, i.e., $\mathrm{m} = 100$, the Bingham-Papanastasiou model approaches the Bingham model. The Bingham-Papanastasiou model is valid for all regions, both yielded and un-yielded. Therefore, it avoids determining the yield surface, which brings important advantages especially for numerical modeling.

3.2 Numerical simulation results

We extended our in-house code FracFlow to directly simulate the Bingham grouts flow in a single rock fracture. The FracFlow code is an unstructured finite volume method code developed to directly solve fluid flow and solute transport in single rock fractures. The detailed numerical schemes can be found in Zou et al. (2015; 2016). A single rough-walled fracture model has been created from a laser-scanned digital surface of a granite rock sample. The detailed statistics of the digital surface and this created fracture model can be found in Zou et al. (2014; 2015). For all simulations, the inlet boundaries are set with constant flow rate, and the outlet boundaries are set with zero pressure. The upper and lower plates are set as no-slip walls, i.e. with zero velocity. The parameters adopted for the numerical simulation are summarized in Table 2.

Table 2 Geometrical and physical parameters adopted for the numerical simulation.

Parameters	Units	Values
Fracture length, L	[m]	0.1
Mean aperture, $2B$	[m]	1e-3
Viscosity of grout, $\boldsymbol{\mu_g}$	[Pa·s]	0.025
Yield stress of grout, $\boldsymbol{\tau_0}$	[Pa]	5
Density of grout, $\boldsymbol{\rho_g}$	[kg/m^3]	1500
Reynolds number, $\mathbf{Re} = \boldsymbol{2Bu\rho_g/\mu_g}$	[-]	0.05, 0.1, 0.5, 1, 5, 10, 50, 100, 500, 1000

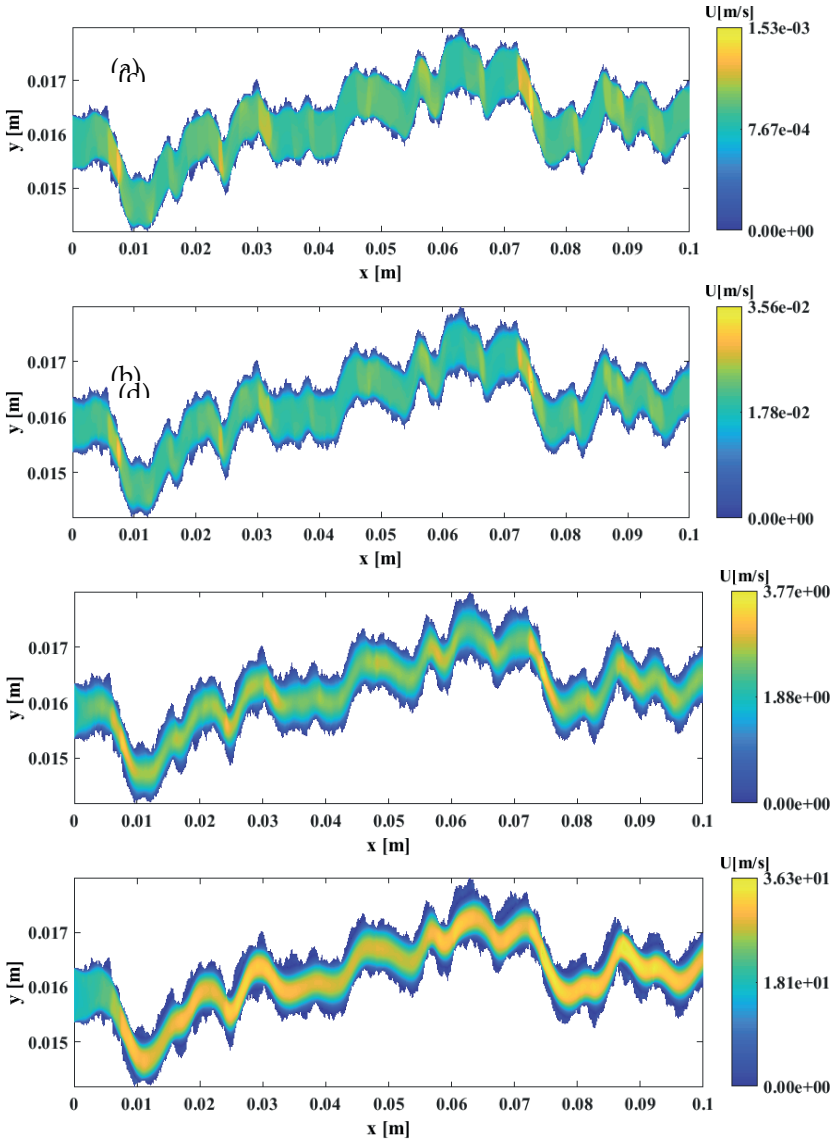

Figure 6 Overview of velocity distribution in the single rough-walled fracture, (a) Re = 0.05, (b) Re = 1, (c) Re = 100 and (d) Re = 1000.

Figure 6 presents representative results of the overall velocity field distributions with Re = 0.05, 1, 100 and 1000, where the contour maps represent the magnitude of the velocity field, i.e., $\sqrt{u^2 + v^2}$. When the Re is relatively small, i.e., $\mathrm{Re} \leq 1$, the high velocity regions are distributed discretely along the fracture where the aperture is relatively small.

In contrast, the low velocity regions are distributed near the rough walls where the aperture is relatively large including sharp cornered asperities of the wall surfaces. When the Re is relatively high $\mathrm{Re} \geq 100$, the high velocity regions are concentrated in the middle of aperture and the relatively low velocity regions become larger than the cases with smaller Re. This result presents the flow behaviors of non-Newtonian grouts in fractures at different Re values.

Figure 7 presents the relationship between the flowrate and the overall pressure gradient for Bingham grout flow in the rough-walled fracture. The theoretical relationship between the flowrate and pressure gradient for the idealized smoothed parallel plates model with the same mean aperture (1mm) is also plotted for comparison (the red curve). The flowrate for the rough-walled fracture by numerical simulation matches well with the theoretical values for the idealized homogeneous fracture when the pressure gradient is relatively small (i.e., $\mathrm{Re} \leq 10$). In contrast, the analytical solution for idealized homogeneous fracture significantly overestimates the flowrate for the rough-walled fracture when the pressure gradient is relatively large (i.e., $\mathrm{Re} \geq 50$).

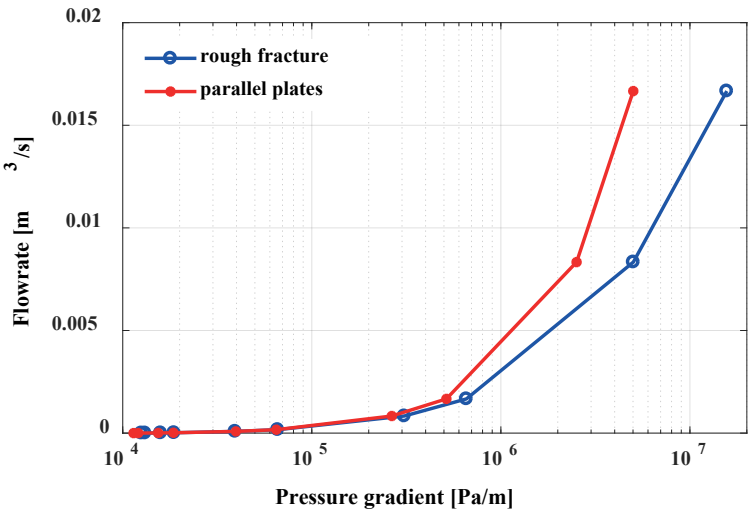

Figure 7 Relationship between the flowrate and overall pressure gradient.

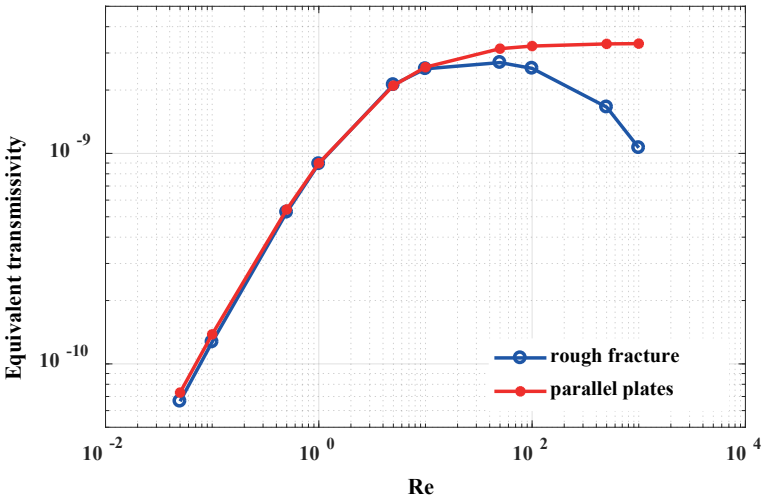

Figure 8 Equivalent transmissivity for different Re.

Figure 8 presents the equivalent transmissivity for different Re. The equivalent transmissivity is calculated based on the relationship between the flowrate and overall pressure gradient shown in Figure 4. The theoretical equivalent transmissivity for the idealized homogeneous fracture with the same mean aperture (1mm) is also presented for comparison (the red curve). Obviously, the equivalent transmissivity is a nonlinear function of Re, where the theoretical transmissivity increases with increasing Re until $\mathrm{Re} \geq 50$ because the yield stress caused plug flows become less important with increasing of Re. For cases with $\mathrm{Re} \leq 10$, the equivalent transmissivity for the rough-walled fracture matches well with that for the idealized homogeneous fracture. It indicates that the fracture surface roughness has limited impact on the equivalent transmissivity when Re is relatively small, where the plug flow dominates the equivalent transmissivity. However, for cases of $\mathrm{Re} \geq 50$, the equivalent transmissivity for the idealized homogeneous fracture approaches a constant value whereas the equivalent transmissivity for the rough-walled fracture decreases with increasing Re, due to the increasing inertial effects. This result indicates that the surface roughness only affect the equivalent transmissivity when Re is relatively large, i.e. $\mathrm{Re} \geq 50$. In grouting, the Re reduces from infinite large to 0 (when grout stops), which covers the full range of Re.

4. Two-phase unidirectional flow in a single fracture

In this Chapter, we present a two-phase flow model for modeling of non-Newtonian cement grouts propagation in a single water-saturated fracture. More details can be found in Zou et al (2018).

4.1 Physical consideration and mathematical model

We consider an immiscible two-phase flow process in a single fracture defined by two smooth parallel plates. Surface roughness or aperture variability are clearly present in natural rock fractures however these are not considered in the present study in order to focus on the effect of water flow.

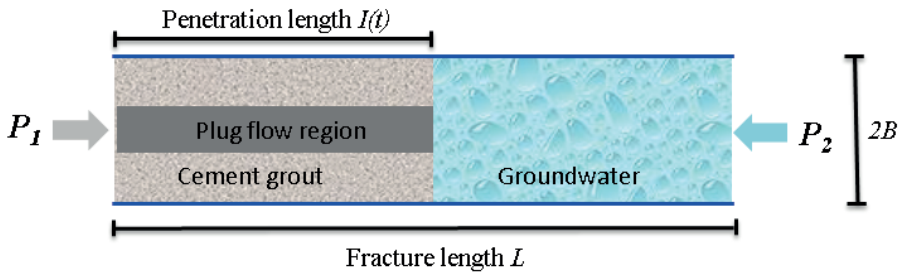

Figure 9 Illustration of cement grout penetration into a single water-saturated fracture.

Figure 9 presents the conceptual model of grouting with immiscible multiphase flow in a water-filled idealized planar fracture, as the basic element of the fracture networks in rock masses. The fracture aperture is 2*B*. The cement grout is considered as a Bingham fluid, injected from the left-hand-side of the fracture (i.e. inlet) with a constant effective grouting pressure P_1, which follows the previous studies and the condition used in the RTGC approach. The length of the fracture is *L*. The water pressure on the right-hand side of the fracture (i.e. outlet) is P_2. In the grouting process, the grout displaces the groundwater in the fracture. The distance between the inlet and the grout front, i.e. the interface between grout and water, represents the grout penetration length *I(t)*, which is a function of the grouting time.

According to the same assumptions for single-phase flow, the grouting process of immiscible two-phase flow in the fracture can be described by a set of the following equations

$$\frac{\partial}{\partial \mathrm{x}} T(C) \frac{\partial \mathrm{P}}{\partial \mathrm{x}} = 0 \tag{36}$$

$$u = \frac{T(C)}{2B} \frac{\partial \mathrm{P}}{\partial \mathrm{x}} \tag{37}$$

$$\frac{\partial C}{\partial t} + u \frac{\partial C}{\partial \mathrm{x}} = 0 \tag{38}$$

where $T(C)$ is the transmissivity which is depending on the phase function. The transmissivity for the Bingham grout can be written as

$$T(C=1) = -\frac{B^3}{3\mu_g}\left(1-\frac{z_p{}'}{B}\right)^2\left(2+\frac{z_p{}'}{B}\right) \tag{39}$$

where μ_g is the viscosity of grout, $z_p{}'$ is half of the plug flow region, determined by the yield stress and the pressure gradient between the injection surface and grout penetration front I(t),

$$z_p{}' = min\left(\frac{\tau_0 \mathrm{I(t)}}{P_1 - P_{I(t)}}, B\right) \tag{40}$$

where $P_{I(t)}$ is the pressure at the interface. For the groundwater, the transmissivity is given by the cubic law, expressed by

$$T(C=0) = -\frac{2B^3}{3\mu_w} \tag{41}$$

where μ_w is the viscosity of groundwater.

Initially, the fracture is filled with water, i.e. $C = 0$, at t = 0. The grout is injected into the fracture through the inlet boundary under a constant pressure P_1, i.e. $C = 1$ and P = P_1 at x = 0 when $t > 0$. At the outlet boundary, P = P_2 and $\frac{\partial C}{\partial x} = 0$ at x = L.

4.2 Solution method

The governing equations (36)-(38) are a set of nonlinear partial differential equations, since the transmissivity of the Bingham grout is a function of the pressure difference and penetration length. A Galerkin finite element method code using the Picard iterative method is developed to solve for the nonlinear Reynolds equation. The FEM - rather than iteratively solving the pressure at the interface by using the flowrate equation - is used because of its advantages in consideration of complex geometry and spatially varying properties of the grout for further studies. At each time step, the mesh is refined by adding one node at the interface, so that only one pressure value is directly solved at the interface node without need for subsequent interpolation; this ensures continuity of the pressure field at the interface. The velocity is then calculated by equation (37) after obtaining a convergent pressure field.

The phase transport is a hyperbolic (advection) equation, which is a difficult numerical problem in the presence of a sharp interface (i.e. high phase gradient) at the grout front if an Eulerian scheme is used. To overcome this numerical difficulty, a Lagrangian interface tracking method was adopted to track the grout penetration. The advective interface transport follows the motion equation and is written as

$$\mathrm{I^{n+1}} = \mathrm{I^n} + \mathrm{u(I^n)\Delta t} \tag{42}$$

where I is the position of the interface and Δt is the time step. Since equation (23) is an explicit discretization scheme, the adaptive time step based on the Courant-Friedrichs-Levy (CFL) condition is used in this study to achieve higher efficiency and maintain computational stability for the solution, expressed by

$$\Delta t \leq \frac{\Delta x}{u} \tag{43}$$

where Δx is a characteristic length assumed to be the mesh size.

4.3 Evolution of the pressure distribution

A series of numerical simulations were conducted to illustrate the grouting process and investigate the importance of the water phase flow. The adopted model geometry and the physical parameters (typically used in rock grouting practice) for the simulation are summarized as follows. Three fracture lengths (i.e., L=10 m, 25 m and 50 m), corresponding to three values of grout yield stress (i.e., τ_0= 5 Pa, 2 Pa and 1 Pa) are used to show the grout yield stress on the sensitivity of penetration process. The fracture aperture is 1 mm. The grouting pressure is 100 kPa. Six values of the grout viscosity (i.e., μ_g= 0.0025 Pa·s, 0.005 Pa·s, 0.01 Pa·s, 0.05 Pa·s, 0.075 Pa·s and 0.1 Pa·s) are adopted for the numerical simulation to demonstrate the impact of grout viscosity. The viscosity of water is 0.001 Pa·s. To evaluate the impacts of water phase flow, simulation results of the two-phase flow are compared with the results of single-phase flow where water phase flow is neglected; the latter case is simulated by setting water viscosity as 1e-10.

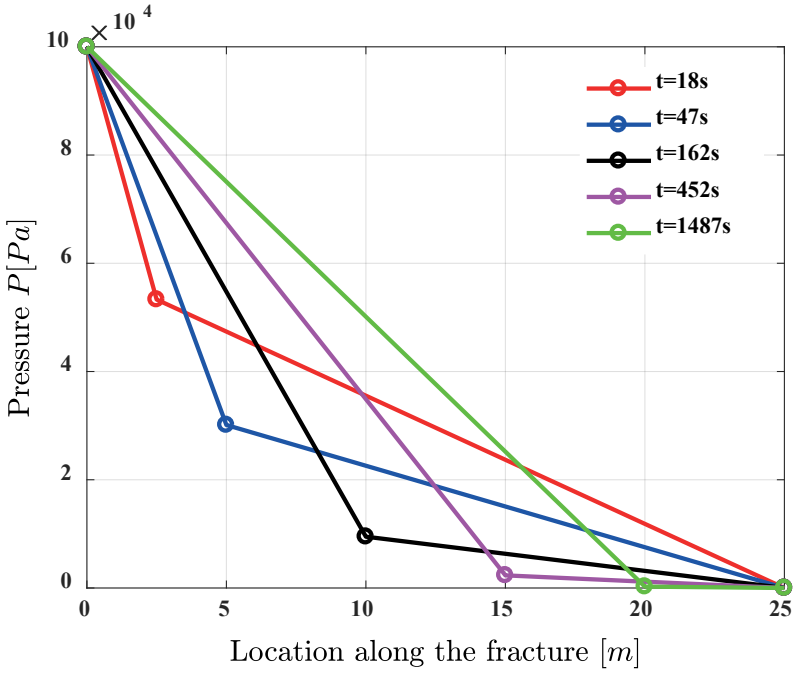

Figure 10 Evolution of the pressure distribution along the fracture, for $\tau_0 = 2\text{Pa}$, $\mu_g = 0.01\text{Pa} \cdot \text{s}$.

Figure 10 presents the evolution of the pressure distribution along the fracture for the two-phase flow, exemplified by the case when $\tau_0 = 2\text{Pa}, \mu_g = 0.01\,\text{Pa} \cdot \text{s}$. The pressure gradients (the slopes of the pressure curve) in the two phases are different, which is caused by the different transmissivity values for the grout and water. The pressure at the interface (i.e. grout penetration front) decreases with the growth of penetration length or the grouting time. In the case of single-phase grout flow, the pressure at the grout front is constant and equal to the in situ groundwater pressure, i.e. $P_2 = 0$ assumed in this study. However, this result shows that the pressure at the front is not constant as $P_2 = 0$. It indicates that the flow of the water phase also importantly leads to the pressure drop, which may be a potential source of uncertainty in application of models that ignore the water phase flow.

4.4 Impact of two-phase flow

Figure 11 presents a comparison between numerical results for two-phase flow and single-phase flow (i.e. in absence of water flow), for different viscosity values of the grout. When the viscosity of grout is relatively small, e.g., $\mu_g = 0.0025\,\text{Pa} \cdot \text{s}$ (red curves), the penetration curves (movement of the interfaces) exhibit significant

discrepancies between the results of two-phase flow and single-phase flow, especially at the earlier stage of grouting. The maximum difference is around 6m (~25% of the fracture length). The discrepancies decrease for the case when viscosity of the grout is relatively large, e.g., $\mu_g = 0.1\text{Pa} \cdot \text{s}$ (black curves). These discrepancies are caused by ignoring the water flow in the simulation of single-phase flow. It demonstrates that the water phase flow may significantly affect the grout penetration process especially when the viscosity of grout is relatively small.

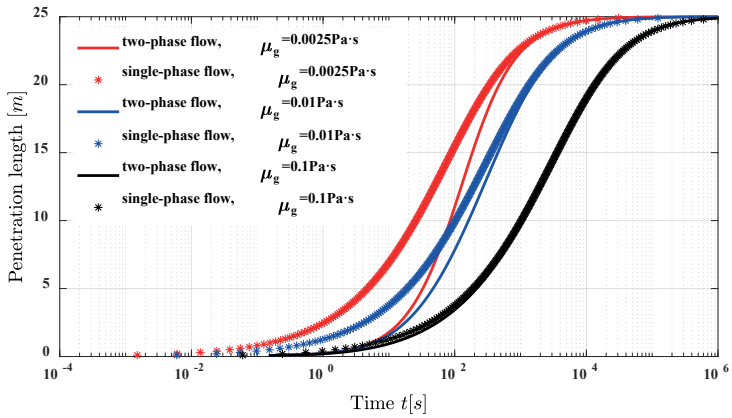

Figure 11 Comparison of simulation results between two-phase flow and single-phase flow, for $\tau_0 = 2\text{Pa}$.

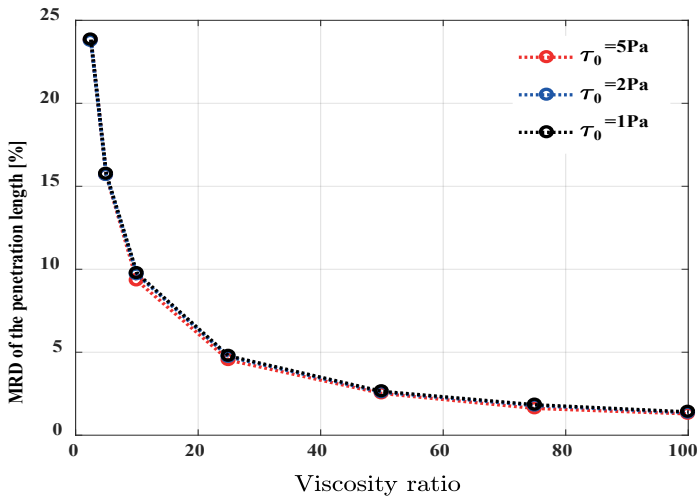

Figure 12 The maximum relative difference (MRD) of the penetration length between the results of two-phase flow and single-phase flow for different viscosity ratios (between grout and water) and yield stresses.

To further quantitatively illustrate the impacts of the water phase flow and analyze the sensitivity of the penetration length to the viscosity ratio between the grout and water, the maximum relative difference (MRD) of the grout penetration length between the results of two-phase flow and single-phase flow for different viscosity ratios and yield stresses are presented in Figure 12. The MRD is defined by

$$\mathrm{MRD} = \frac{max(I_i^s - I_i^t)}{I_{max}} \times 100\% \tag{44}$$

where I_i^s and I_i^t is the grout penetration length for two-phase flow and single-phase flow, respectively, I_{max} is the maximum penetration length determined by the yield stress, pressure and aperture. The larger values of the MRD imply higher importance of the water phase flow.

At a given grouting time, the normalized MRD of the penetration length between numerical and analytical results decreases from ~25% to less than 2% when the viscosity ratio between the grout and groundwater increases from 2.5 to 100. This result quantitatively demonstrates the impacts of the two-phase flow effects, which significantly depends on the viscosity ratio between the grout and groundwater. The typical viscosity ratio in rock grouting practice is around 20 (i.e., the grout viscosity is around 0.02 Pa·s), and the effect of two-phase flow is still significant. Using models that ignore the water phase flow will overestimate the penetration length, especially at an early stage of grouting.

The MRD is insensitive to the yield stress of the grout, indicating that the impact of the water phase flow is independent of the grout yield stress. However, the yield stress will affect the absolute differences between the two-phase flow and single-phase flow, since the yield stress determines the maximum penetration length of the grout.

4.5 Impact of water flow under grout hardening

Due to physical and chemical processes, the cement grout properties (e.g., viscosity and yield stress) increase with time, known as the hardening process. Both linear functions and exponential functions have been used to model the hardening process for cement/bentonite grouts by Håkansson (1987; 1993) and Hässler (1991). In this study, an exponential function is also adopted to describe the time-dependent viscosity and yield stress, written as,

$$\mu_g(t) = \mu_I e^{at} \tag{45}$$

$$\tau_0(t) = \tau_I e^{bt} \tag{46}$$

where μ_I and τ_I is the initial viscosity and yield stress, a and b is a parameter controlling the increase rate (i.e. hardening rate) of viscosity and yield stress of the grout, respectively.

In this study, the initial viscosity $\mu_I = 0.01\text{Pa} \cdot \text{s}$ and the initial yield stress $\tau_I = 2\text{Pa}$ are adopted for the simulation. To illustrate the sensitivity on the hardening rate, three sets of parameter a and b, representing low (a = 0.00025 and b = 0.0002), median (a = 0.0005 and b = 0.0004) and high (a = 0.00075 and b = 0.0006) hardening rate are simulated. By considering the three cases of the hardening process, the penetration lengths for the two-phase flow and the single grout flow are calculated to demonstrate the significance of water flow, presented in Figure 13.

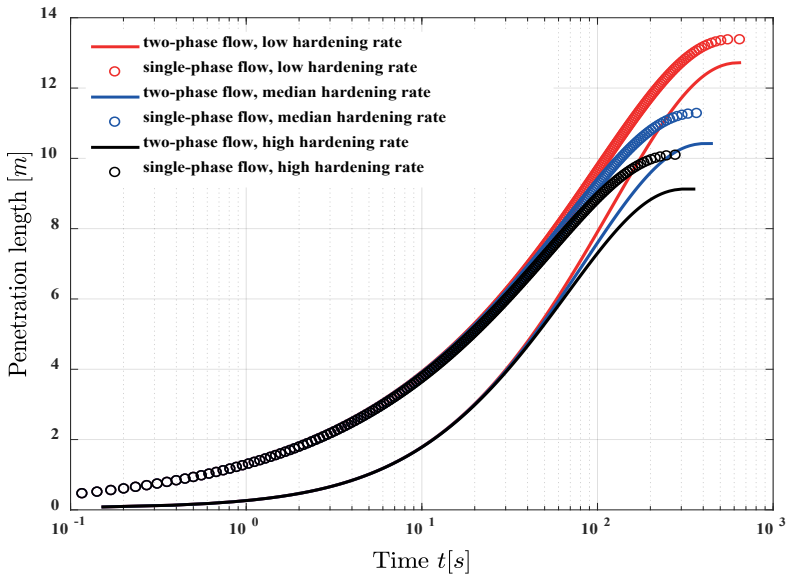

Figure 13 The penetration lengths for the two-phase flow and the single-phase flow under different conditions of grout hardening rate.

Under the condition of grout hardening, the penetration lengths for the two-phase flow and the single-phase flow exhibit more significant differences compared to that without considering the hardening process (see Figure 13). The results of single-phase flow by ignoring the water flow generally overestimate the penetration length not only for the early stage but also for the entire grouting process until it stops. This is caused by the time-dependent viscosity and yield stress of the grout that enhances the differences between the two cases (i.e. the two-phase flow and the single-phase flow) with grouting time. This result indicates that the water flow has a more significant impact under the realistic conditions that includes the grout hardening process. In addition, the hardening process significantly affects the penetration length for relatively longer grouting time

before the grout stops, due to the increase of viscosity and yield stress. The maximum penetration lengths reduce with the increasing hardening rate.

5. NON-NEWTONIAN GROUT PROPAGATION IN 2D FRACTURE NETWORKS

In this Chapter, we present validation results for the extended two-phase flow model for cement grouts propagation in 2D fracture networks. Using the validated model, we studied the impact of fracture structure, hydraulic variability and rheological properties on grout propagation process. More details can be found in Zou et al (2019a; 2019b; 2020).

5.1 Mathematical model and solution method

To extend the two-phase flow model to the DFN system, the Reynolds equation (1) needs to be integrated over the network based on the connectivity between each single fracture, expressed as

$$\int \frac{\partial}{\partial \mathrm{x}} T(C) \frac{\partial \mathrm{P}}{\partial \mathrm{x}} dx = \sum T(C) \frac{\partial \mathrm{P}}{\partial \mathrm{x}} = 0 \tag{47}$$

which represents mass balance over the DFN system. Together with equations (37) and (38) for calculating the velocity and phase transport equation in each single fracture, Equation (47) defines the basic mathematical model for two-phase flow in a DFN system. The mathematical model for two-phase flow in a DFN system is based on the theory for the same in a single fracture. The main differences and difficulties encountered when extending the two-phase flow model from a single fracture to fracture networks are dealing with the integration of the mass balance equation (47) and solving the phase transport equation (38), for each discrete fractures in the network.

Due to the nonlinearity of the mathematical model and complexity of the DFN structure, equations (47) can only be solved numerically through iteration at each time step. Equation (47) is equivalent to applying a finite volume method to solve equation (36) over each single fracture, which represents the local mass balances at each fracture segment formed by the lines between each two adjacent intersection nodes in a fracture.

We introduce a moving node in each fracture to track the propagation of propagation interface. For any node *i* including the moving nodes in the entire network, equation (47) can be discretized as

$$\sum_{j=1}^{M} [T(C)]_{ij} \frac{P_j - P_i}{L_{ij}} = 0 \tag{48}$$

where M is the number of neighboring nodes, and L_{ij} is the length between the nodes *i* and *j*. Assembling the discretized equation (48) over all fractures (referred to volumes or cells in the finite volume method) yields a system of nonlinear equations, which can be solved by using iteration methods. The Lagrangian interface tracking method is used to track the grout propagation fronts (see equation 42).

The detailed algorithm of the solution for the two-phase flow of grout propagation in saturated fracture networks is summarized as follows:

a) Define the rheological parameters of the grout (yield stress, τ_0, and plastic viscosity, μ_g), the controlling parameters (injection pressure, P and the maximum injection time, t_{max}), the DFN structure and the hydraulic information (fracture apertures, b).

b) Initialize the phase function C and the pressure field P_0, for t = 0.

c) Determine the transmissivity $T(C)$ for each fractures according to the phase function and the pressure field, based on equations (39-41).

d) Compute the new pressure field P_1 by solving equation (48).

e) Compare the new pressure field P_1 with the previous pressure field P_0: if the difference meets the convergence condition$max\ (|P_1 - P_0|) < \varepsilon$, where ε is a small number representing the error tolerance, then go to f); otherwise, let $P_0 = P_1$ and go back to c).

f) Compute the velocity u according to equation (37) and determine the time step Δt according to equations (43).

g) Update the location of the interface through point tracking based on equation (42) and $t = t + \Delta t$.

h) Stop criteria: if $t < t_{max}$, go back to c); otherwise, finish and stop.

5.2 Verification by experimental data

To verify the two-phase flow model and the proposed computing algorithm for a fracture network, simulation results are compared with experimental data obtained in a laboratory test system (Figure 14) (Håkansson 1987). The experiment of Håkansson (1987) is considered as a benchmark in the literature (e.g. Hässler 1991; Eriksson et al. 2000; Mohajerani et al. 2017) mainly because they were conducted on a relatively large scale relevant for fractured rock applications.

This test system consists of two parallel plates of plexiglass with the size of $1.2 \times 1 \times 0.015$ m. The two sides along the length of the plates were sealed and the remaining two sides along the width of the plates were fixed by given water heads. One hundred and twenty rectangular plexiglass plates were homogeneously placed between the two plates to construct the regular fracture network. The fracture aperture is 1 mm and the width of the fractures is 5 mm. At the center of the top plate, a circular hole was drilled for injecting a non-Newtonian fluid.

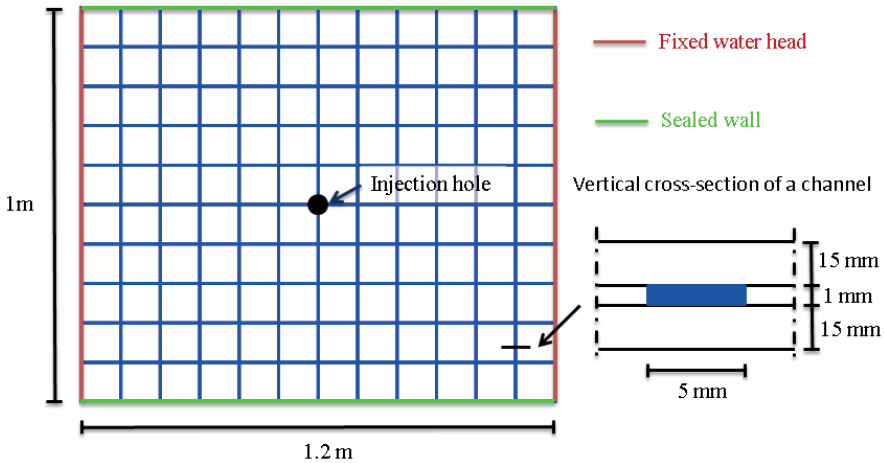

Figure 14 Schematic illustration of the laboratory test system.

In this experiment, all fractures were initially filled with water. The injected non-Newtonian fluid was a bentonite grout, characterized by a rheometer and fitted to the Bingham model. The curve fitted yield stress was 3 Pa and the viscosity was 0.035 Pa · s; the injected fluid had time constant rheological properties. The injection pressure forcing the fluid displacement was 4.8 kPa and the entire propagation process was filmed by a camera placed orthogonally above the transparent experimental plate. The video of the test, which contains the entire dataset of the propagation time and positions, is presented in the Supplement Material. Specific snapshots from this experiment have been considered in the literature (e.g. Hässler 1991; Eriksson et al. 2000; Mohajerani et al. 2017), however the full and continuous experimental dataset is presented for the first time in this study.

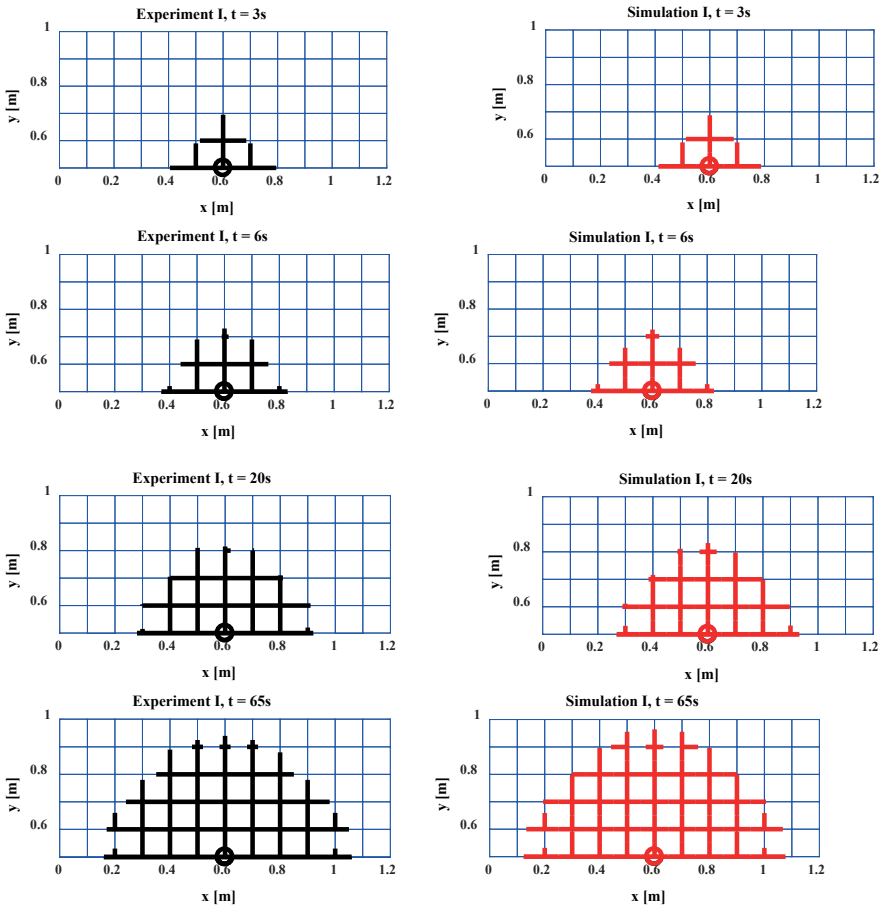

Figure 15 Comparison of propagation patterns between experiments and simulations at t = 3s, 6s, 20s and 65s.

Figure 15 shows comparison of injected fluid propagation in the fracture network for different times, i.e. t = 3s, 6s, 20s and 65s, between experimental results and numerical simulations. Only the top half of the fracture networks are shown due to symmetry. With increasing time, the injected fluid gradually displaces the water in the fracture network. Simulated result matches very well with the experimental data for all the times. This indicates that the two-phase flow model developed in this study is sufficiently accurate and can be used for modeling two-phase flow of yield-power-law fluids propagation in an advection-dominated, water-saturated fracture network. Compared with the results presented in previous studies (e.g., Hässler 1991; Eriksson et al. 2000; Mohajerani et al.

2017), simulation results presented in this study (Figure 15) better match the experimental data, indicating that the mathematical model and solution method are more accurate.

To quantitatively compare and follow the evolution of the propagation process, a parameter representing the volume fraction between the penetrated volume and the total volume of the fractures is defined. Specifically, a penetration volume fraction is

$$\Gamma = \frac{V_p}{V_c} \tag{49}$$

where V_p is the penetrated volume and V_c is the total volume of the fractures.

Figure 16 shows the evolution of the penetration volume fraction Γ from the numerical simulation result. The experimental result is also presented for comparison, which matches well with the simulation result. The penetration volume fraction Γ increases rapidly in the initial phase and gradually slows down with increasing time, especially after 120s when the injected fluid arrives at the sealed walls; this is caused by the gradually reduction of the pressure gradient in the fractures and the yield stress of the injected fluid.

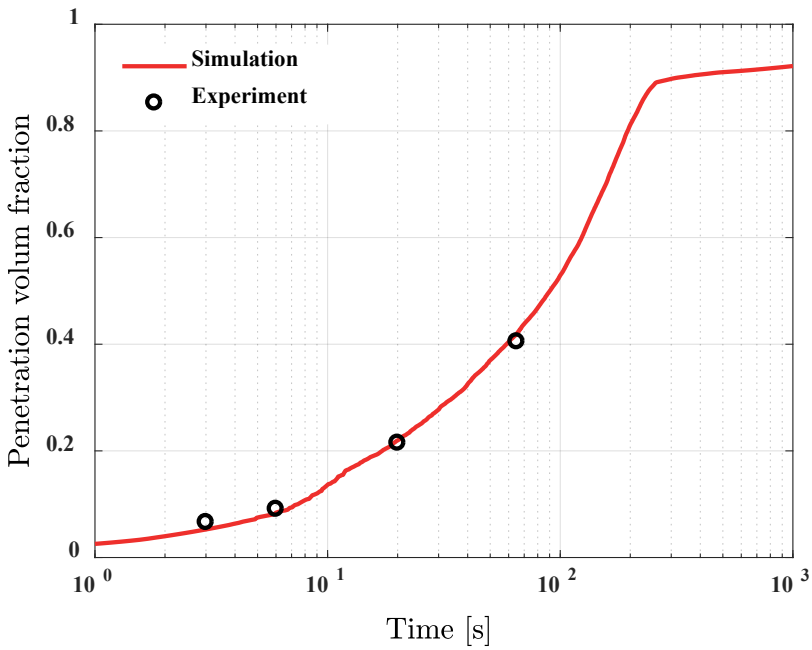

Figure 16 Comparison of penetration volume fraction between the simulation results and experimental data.

5.3 Fracture network generation and simulation setting

In this study, randomly generated 2D DFN models based on cumulative density functions of location, orientation and size of fractures, are used to illustrate two-phase cement grouts propagation in rock fracture networks. A similar approach for generating 2D DFN models can be found in the literature (e.g., Baghbanan and Jing 2007). In this study, the cumulative density functions and associated parameters used for generating the DFN model are based on site investigation data inferred from Forsmark (Sweden), a potential site for Swedish radioactive nuclear waste disposal. The parameters, distributions and values used to generate the DFN for this study are summarized in Table 3.

Table 3 Distributions and parameters used to generate the DFN model.

Domain size	10m×10m
Fracture sets	5
Density	1.2
Location	Uniform distribution
Orientation	Fisher distribution
	Trend/plunge: 292/2, 326/2, 60/6, 15/2 and 5/86
	Fisher constants: 17.8, 14.3 12.9, 14.0 and 15.2
Lengths	Fractal
	(minimum 1 m, maximum 564 m, fractal dimension 1.2)
Width	0.5 m
Aperture	Truncated lognormal distribution
	(minimum $1\ \mu m$, maximum $200\ \mu m$, mean $\bar{b} = 100\ \mu m$, standard deviation $\sigma = 0, and\ 1$)

To quantify the impact of the network structure, 50 DFN realizations are generated using the same values of the distribution parameters. The number of realizations is chosen by a convergence analysis of the propagation results, to ensure that the number of realizations is sufficient for obtaining stable results. Figure 17 exemplifies one generated DFN, illustrating the complex fracture networks.

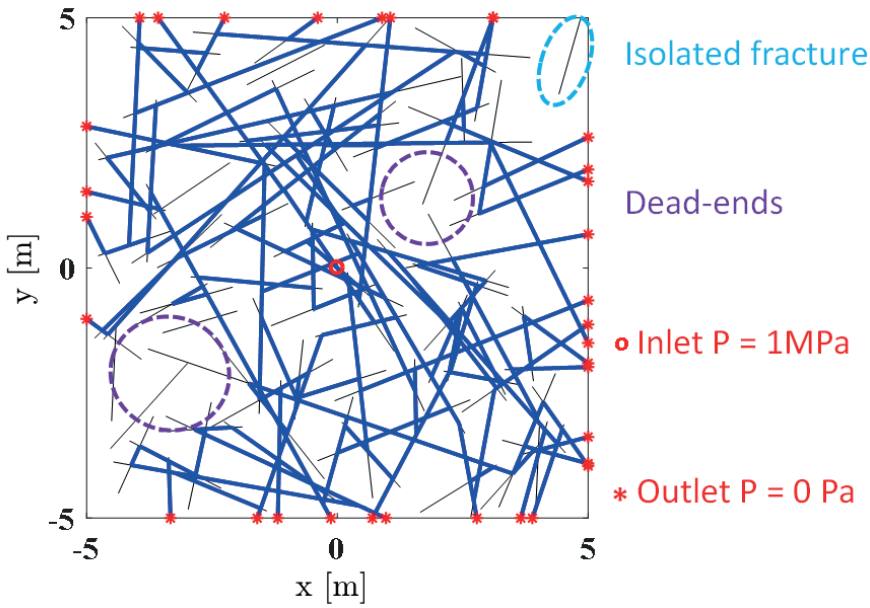

Figure 17 A random generated DFN realization by using the distributions and parameters provided in Table 3.

It is well known that the fracture hydraulic apertures are highly heterogeneous and may vary significantly between fractures, which often follows the truncated power-law distribution (Renshaw and Park 1997) or the truncated lognormal distribution (Dverstop and Andersson 1989; Pyrak-Nolte et al. 1997). The truncations are due to the limitation of measurement for small apertures. In addition, the fracture aperture might be correlated to the fracture length, where the longer fractures exhibit larger apertures (Renshaw and Park 1997; Baghbanan and Jing 2007). Aperture distributions and correlation to lengths were partially confirmed by laboratory or field measurements of single fractures, borehole cores and outcrops (Wang et al. 1988; Renshaw and Park 1997). The distribution of fracture aperture constitutes the main hydraulic variability of the fracture networks in the grouting processes. In order to illustrate the impact of such hydraulic variability on the propagation of cement grouts, two cases of heterogeneous aperture will be considered, one using a truncated lognormal distribution uncorrelated to fracture length, and one perfectly correlated to the fracture length.

The truncated lognormal distribution for the fracture aperture has four parameters, including the lower and upper aperture limits, i.e. b_{min} and b_{max}, and the mean and standard deviation of the aperture natural logarithm, i.e. $\overline{b}$ and σ. The variability of the lognormal distribution is controlled by the parameter σ. Two sets of 50 DFN models, one with a constant aperture $\sigma = 0$ and the other with heterogeneous aperture $\sigma = 1$ are simulated in this study.

For comparison and to highlight the impact of irregular network structure, the case for a structured orthogonal network similar to Hässler (1991) and Hässler et al (1992) with the same size (100 m^2) and the same mean intensity (with 15 orthogonal fractures along horizontal and vertical directions, respectively) as the 50 random DFN models is simulated. To isolate the impact of network structure, the same constant fracture aperture b = 100 μm is adopted in the simulation for this structured network.

Initially, the fracture networks are saturated with groundwater. The grout assumed as a Bingham fluid is injected with a constant pressure (P = 1 MPa) at the center of the network (see Figure 17); note that a deterministic fracture is added at the center to keep the same injection boundary condition for all realizations. The outlet boundary condition is P = 0 Pa, for this generic study (see Figure 17). In practice, the outlet boundary condition is determined by the *in situ* static water pressure in the grouting area. The physical parameters of the Bingham model adopted for all simulations are selected according to typical cement grouts used in practice (Håkansson 1993; Stille 2015). Specifically, the yield stress is 2.5 Pa and the plastic viscosity is 0.025 $\mathrm{Pa \cdot s}$. For groundwater, the viscosity is 0.001 $\mathrm{Pa \cdot s}$. All realizations are conducted by using the algorithm presented in Section 2.2, on a desktop computer. Each realization for the maximum injection time t = 1800 s takes around 20 minutes.

5.4 Grout propagation in 2D fracture networks

Figure 18 shows an example of grout propagation patterns in a DFN system at different times, i.e. t = 450 s, 900 s, 1350 s and 1800 s. In this example, the aperture is constant (b = 100 μm). The grout (marked by red) generally spreads along the connected fractures (marked by blue) after injection. With the injection time increasing from 450 s to 1800 s, the grout gradually fills the connected fractures. However, the rate of filling is different in each fracture. Most well-connected fractures are filled relatively rapidly whereas a few fractures are less penetrated, depending on local pressure gradient affected by the network geometry conditions.

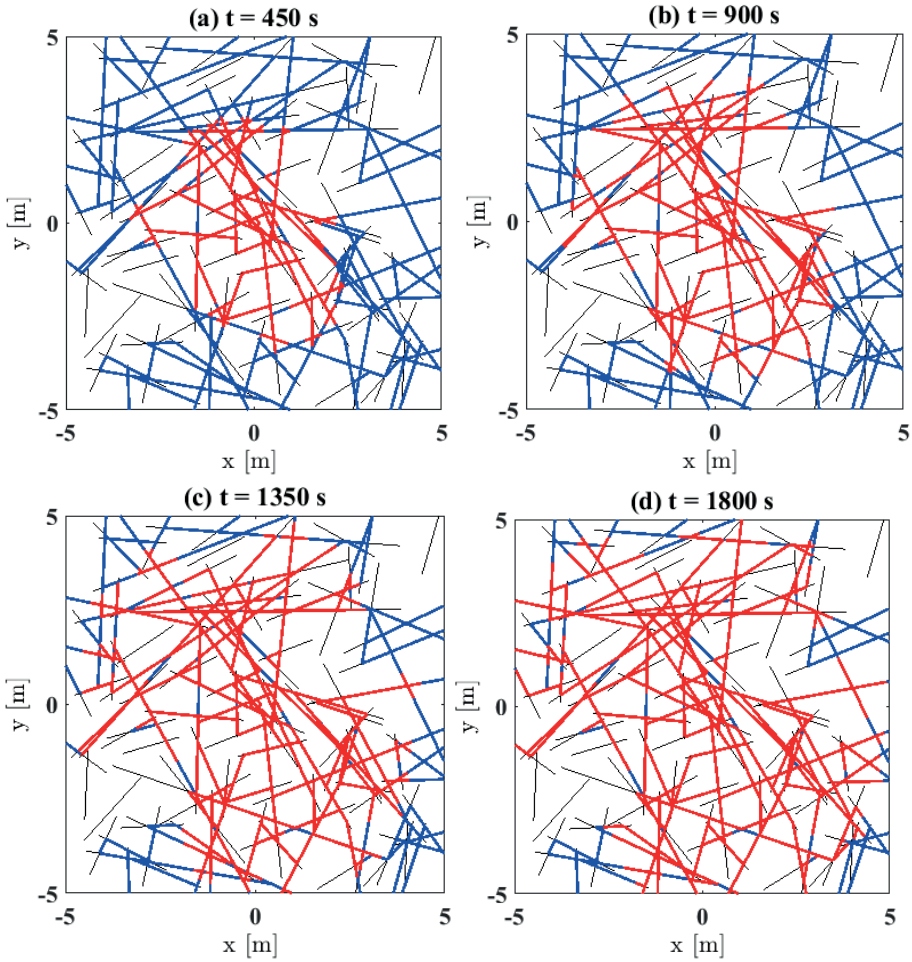

Figure 18 Overview of grout propagation patterns in a DFN with constant aperture b = 100 μm at different times (a) t = 450 s; (b) t = 900s; (c) t = 1350 s and (d) t = 1800 s.

Figure 19 presents the pressure field evolution in the exemplified DFN system at different times, i.e. t = 450 s, 900 s, 1350 s and 1800 s. Generally, the pressure reduces radially around the injection borehole located at the center of the DFN. With the injection time increasing from 450 s to 1800 s, the pressure at the interface (i.e. grout penetration front, see Figure 19) gradually decreases. The pressure values in the cement grout are much larger than that in the water phase, indicating that the pressure drop in the DFN system is mainly caused by the cement grout flow.

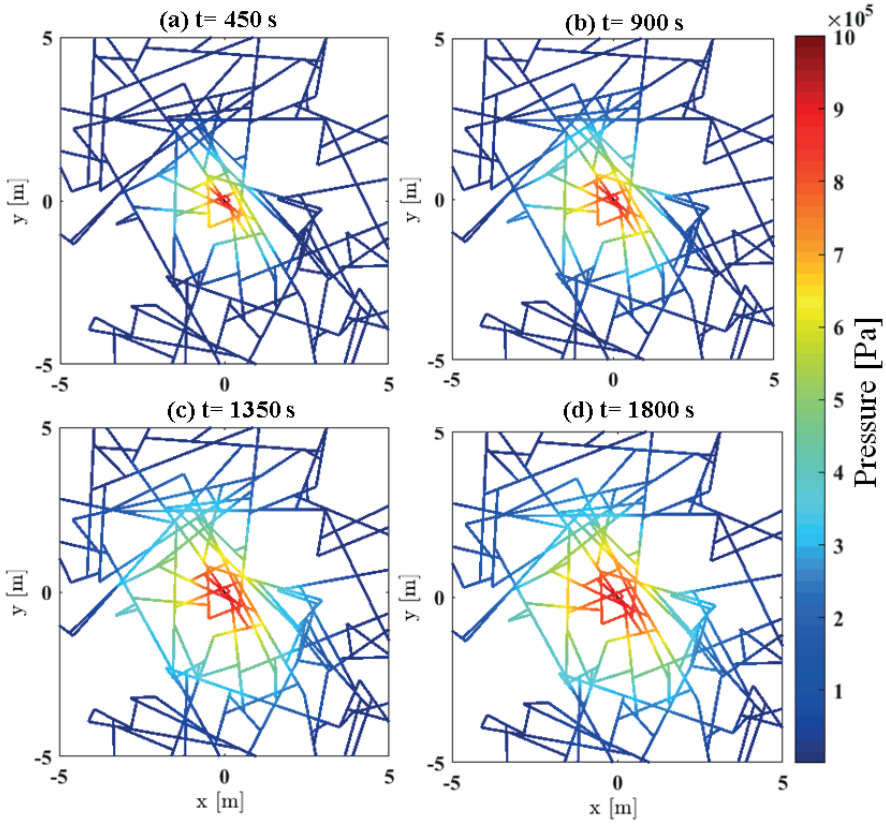

Figure 19 Overview of the pressure field evolution in a DFN with constant aperture b = 100 μm at different times (a) t = 450 s; (b) t = 900s; (c) t = 1350 s and (d) t = 1800 s.

5.5 Impact of network structure and hydraulic variability

To illustrate the impact of network structure and hydraulic variability, the mean of Γ curves of the 50 realizations are analyzed.

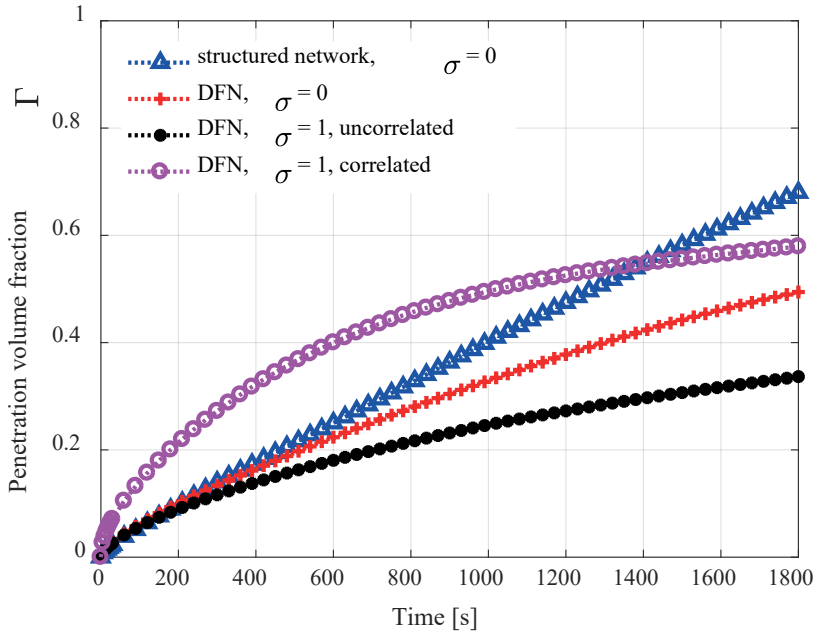

Figure 20 Mean penetration volume fraction Γ curves for different conditions of fracture networks and apertures.

Figure 20 presents the mean Γ curves for different conditions of the fracture network and apertures. Generally, the mean Γ for all cases increases by different rates with time. The simplest reference case is the structured orthogonal network with constant aperture (i.e. $\sigma = 0$), where the mean Γ achieves 0.69 at t = 1800 s (see the blue curve in Figure 20). For the DFN case with the same constant aperture, the mean Γ increases relatively slower and it attains 0.5 at t = 1800 s (see the red curve in Figure 20). Compared to the reference case of a structured orthogonal network with homogeneous aperture, the mean Γ reduces to around 27.5% at t = 1800 s. This implies that the network structure is significant by delaying the grout propagation process.

When the DFN features uncorrelated heterogeneous apertures following the truncated lognormal distribution, $\sigma = 1$ (see the black curve in Figure 20), the increase of mean Γ becomes slower and its value is around 0.37 at t = 1800 s. It reduces 26% compared to the case when the aperture is constant, indicating that the uncorrelated heterogeneous aperture and hydraulic variability also significantly affects the grout propagation process by delaying the propagation. For the case with heterogeneous apertures correlated to the fracture length (see the magenta curve in Figure 20), the mean Γ increases much faster than the other DFN cases during the entire stage of injection, especially compared to the case with uncorrelated heterogeneous apertures. The value of mean Γ is around 0.59,

which is around 60% higher than the uncorrelated case and 18% higher than the case with constant aperture. Such important differences indicate that the correlations between aperture and fracture size may significantly affect the grout propagation processes. The main reason is that the longer fractures have higher transmissivity and better connectivity for the correlated case, which largely enhances the propagation rate. In practice, cement grouting is expected to be more efficient in fracture networks when the aperture is correlated to its size.

5.6 Impact of rheological properties

In order to demonstrate the impact of rheological properties on non-Newtonian grouts propagation in fracture networks, two sets of simulations by varying the yield stress and plastic viscosity are conducted, respectively, using a same random generated network structure.

Figure 21 presents the penetration volume fraction Γ curves for different values of yield stress. Generally, the Γ for all cases increases at different rates with time. The propagation rate gradually reduces when the yield stress increases from 0.5 Pa to 5 Pa. The Γ for the case when yield stress is 0.5 Pa is around 0.55 at t = 1800 s (see the black curve in Figure 21). It reduces around 10% and 13 % for the case when the yield stress is 2.5 Pa and 5 Pa, respectively. This result implies that the yield stress has limited impact on the grout propagation rates in fracture networks, e.g., at 1800 s, the differences of penetration volume fraction is less than 10 % between the cases when yield stress is 0.5 Pa and 5 Pa.

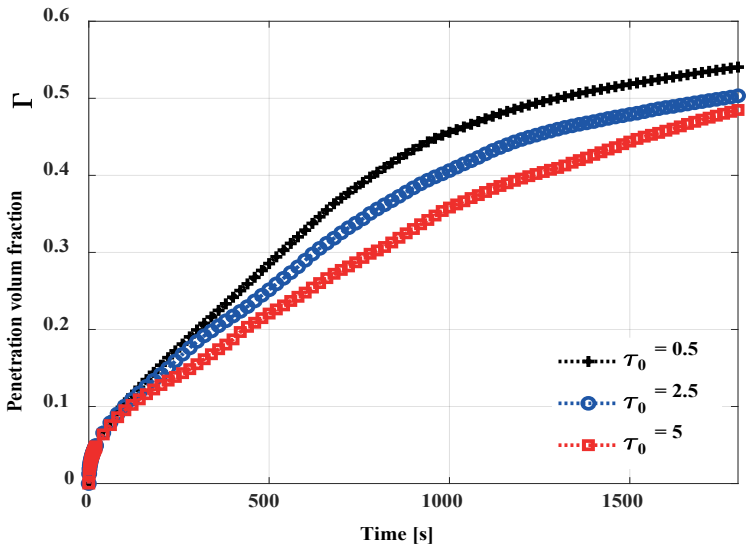

Figure 21. Penetration volume fraction Γ curves for different values of yield stress. The plastic viscosity is 0.025 Pa·s.

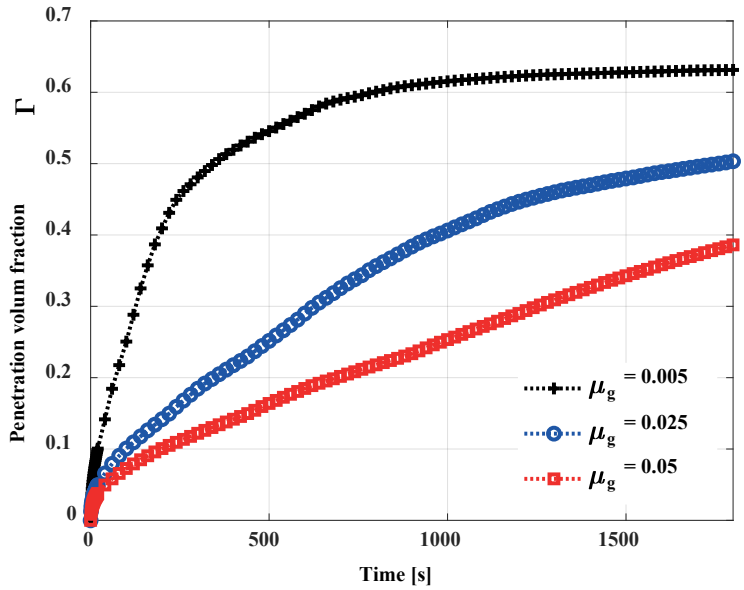

Figure 22. Penetration volume fraction Γ curves for different values of plastic viscosity. The yield stress is 2.5 Pa.

Figure 22 shows the penetration volume fraction Γ curves for different values of plastic viscosity. When the plastic viscosity is relatively small, i.e., 0.005 Pa·s, the grout propagates fast and the Γ approaches 0.64 at t = 1800 s. The propagation rate reduces dramatically with the increase of plastic viscosity from 0.005 Pa·s to 0.05 Pa·s. This result indicates that the plastic viscosity of cement grout significantly influences the propagation processes in fracture networks.

6. CONCLUSIONS

The most important conclusions from this project are summarized as follows:

- For 2D radial flow of a Bingham fluid, the solution presented in this report and the solution by Dai and Bird (1981) are based on different assumptions, that is, Dai and Bird (1981) considered the vertical velocity component in the continuity equation, and we assumed that vertical velocity is negligible. This difference leads to two different approximation models for rock grouting analysis, i.e., one is presented in this report and the other one is derived by Gustafson and Claesson (2005).

- The shape of the plug flow region varies in the two different approximation models, that is, the plug flow region in the model presented in this report is independent of the radius; in the model presented in Dai and Bird (1981) and Gustafson and Claesson (2005), the plug flow region increases with the radius. The reason for the obtained different shapes of plug flow region in the two approximation models is due to the application of different boundary conditions for the shear stress. We use the boundary condition on the surface of the plug flow region, while the other model sets shear stress equal to zero in the middle of the fracture aperture in the plug flow region. Since the two models are zero-order approximation of the realistic kinematical effects and the Bingham model is an idealized rheological model, the real shape of the plug flow region for realistic fluids/grouts remains unknown at this point.

- Using the solution with radius-independent plug flow region presented in this report, the grout penetration length, injected volume and flowrate evolution with respect to the grouting time under constant effective grouting pressure are derived. The closed-form solution of flowrate evolution as a function of grouting time is presented in this study for the first time. These evolution functions provide fundamental theory for rock grouting design and monitoring.

- The differences in the results of grout penetration length and flowrate evolution with respect to the grouting time between the two solutions are negligible within the full range of grouting time.

- The fracture surface roughness significantly affects the local flow behavior for Bingham grout flow in rough-walled rock fractures. The local velocity profiles, as shown in Figure6, cannot be well predicted by the analytical solution based on an idealized smoothed parallel plate model.

- When the Reynolds number is relatively small, i.e., $Re \leq 10$, the surface roughness has limited impact on the overall flow behavior since the flow is controlled by the yield stress for $Re \leq 10$. When the Reynold number is relatively large, i.e., $Re > 10$, the equivalent transmissivity for the rough-walled fracture

reduces with increasing Re. Using the analytical solution will overestimate the realistic transmissivity when Re > 10.

- The water flow significantly affects the pressure distribution in the fracture and delays grout penetration. The impact of the water phase flow is independent of the grout yield stress, but significantly depends on the viscosity ratio between the grout and groundwater, more so for the cases with smaller viscosity ratios.

- The grout hardening process enhances the significance of water flow for the entire grouting time. It is more important to consider the two-phase flow process in modeling of grout penetration under the condition of grout hardening. The penetration length reduces with an increasing hardening rate.

- Analytical solutions or numerical models for rock grouting that ignore water phase flow, e.g., RTGC method, may only be applicable for cases where the grout viscosity is much higher than that of groundwater and the density is close to that of groundwater. Neglecting groundwater in grout flow modeling overestimates the penetration length, i.e. the errors can be over 20% of the maximum penetration length for the cases with low viscosity ratios.

- The two-phase flow model for a single fracture can be extended for modeling of cement grouts as Bingham fluids propagation in 2D water saturated, randomized DFN. The network structure significantly affects grout propagation in fracture networks by delaying the propagation processes. Compared to the structured orthogonal network, the network structure of randomized DFN reduces 27.5% of the penetration volume fraction on average at t = 1800 s, with increased uncertainty with time.

- Features of hydraulic variability, i.e., distribution of apertures, significantly influence the penetration volume fraction of cement grouts. Compared to the case with constant aperture, the penetration volume fraction at t = 1800 s reduces 26% in the case with uncorrelated heterogeneous aperture. The feature of uncorrelated heterogeneous aperture also significantly increases the variability range and standard derivation of the penetration volume fraction.

- Correlation of aperture to the fracture length is another feature of hydraulic variability that significantly affects the propagation processes. The length-correlated heterogeneous aperture largely increases the propagation rate and reduces variability range compared to the uncorrelated case.

- The rheological properties of the cement grout, i.e., yield stress and plastic viscosity, significantly affect the propagation process of cement grout in discrete fracture networks. The propagation rate gradually reduces when the yield stress increases from 0.5 Pa to 5 Pa. The penetration volume fraction at t = 1800 s reduces around 10% and 13 % when yield stress increase from 0.5 Pa to 5 Pa. The propagation rate reduces dramatically with the increase of plastic viscosity. When

the plastic viscosity increases from 0.005 Pa·s to 0.025 Pa·s, the penetration volume fraction at t = 1800 s reduces 23%, and it further reduces 20% when the plastic viscosity increases from 0.025 Pa·s to 0.05 Pa·s.

7. SUGGESTIONS FOR ENGINEERING PRACTICE

To fulfill the general objective of this project that is to improve predictions, design and execution of rock fissure grouting, we conducted a series of theoretical and numerical studies on the cement grout propagation in single fractures and fracture networks. Those theoretical and numerical studies are important bases for improving best practice regarding predictions, design and execution of rock grouting, even though we have not start to work with field data in this project. According to the conclusions drawn from our theoretical and numerical studies, the following suggestions for engineering practice are summarized below:

- From a practical point of view, the differences in prediction results between the two solutions are negligible, so that both solutions can be used for rock grouting analysis in practice. However, the expression of the solution with radius-independent plug flow region presented in this report is much simpler than the solution by Gustafson and Claesson (2005). Therefore, it is recommend using the solution including the evolution of injected grout volume presented in this report for prediction, design and execution of rock grouting in practice for simplicity.

- At present, the fracture surface roughness has not been directly considered in current analytical models used in practice, e.g., RTGC method. Meanwhile, parameterization of fracture surface roughness remains a challenge since it is difficult to access the fracture surface roughness data in the field. Nevertheless, for rock grouting design, ignoring the impact of fracture surface roughness may overestimate the penetration length, especially at the initial stage of injection where the Reynolds number is high. Meanwhile, in practice, proper characterization of the aperture variability by hydraulic tests is very important for accurately prediction of grout propagation in fractured rocks.

- The groundwater flow driven by the injected grouts in the rock grouting process is ignored in most analytical models used in practice, e.g., RTGC method. Since the water phase flow significantly affects the pressure distribution in the fracture and delays grout propagation, we recommend considering the water flow process and using the two-phase flow in the design of rock grouting, especially when the grout viscosity is relatively small that close to the water viscosity.

- The extended DFN model provides an efficient numerical tool for quantifying rock grouting in fractured rocks. Compared to current analytical models based on the assumption of idealized single fractures, the DFN models accounts for the more realistic geological conditions of the fractured rocks. Therefore, we recommend further developing and using DFN models to conduct real-time prediction and controlling in practice.

- We have shown that the rheological properties of the cement grout significantly affect the propagation rate. In practice, accurate measurement for rheological

properties of the cement grout is required for more accurately prediction of grout propagation in fractured rock. We recommend using real-time measured rheological properties for predictions, design and execution of rock grouting in practice.

8. FUTURE STUDY

Although the results obtained in this project led to some important findings in theoretical and numerical modeling of rock grouting, many open questions and challenging issues remain due to both complex geometric conditions of natural rock fractures and complex rheological properties of grouts. The following studies are recommended for the future:

- We only illustrated the general impact of rheological parameters on the grout propagation in rock fractures. The physical and chemical properties of grout materials and additives and their impacts on rheological properties, e.g., time-dependent yield stresses and viscosities, are required to be further studied for specific grouts (with or without specific additives) in order to improve the accuracy for predictions, design and execution of rock grouting in practice (e.g., Zhang et al, 2017; Zhang et al, 2018; Jin et al, 2019; Bahman et al, 2019).
- Currently, we mostly focused on the grout propagation process without consideration of the hydro-mechanical coupling effects. In fact, the injected grout may cause elastic or elastic-plastic jacking or dilation of the fractures, which would consequently affect the propagation process (e.g., Rafi and Stille 2014; Zou et al. 2018). To date, the impact of jacking is only demonstrated in idealized configurations, i.e., smoothed parallel plate models. Such hydro-mechanical coupling effect under more realistic conditions is an important topic that needs to be further studied in the future.
- Our two-phase flow model has been validated by the benchmark experimental data (Håkansson 1987). Further development and validation of theoretical and numerical models requires both reliable laboratory experimental data and high-quality field test data. Therefore, experimental tests with consideration of more realistic conditions, e.g., surface roughness and realistic stress conditions, are important topics for the future study (e.g., Ghafar et al 2017).
- We only simulated grouts propagation in 2D fracture networks. In reality, rock fractures are all distributed in 3D space. Therefore, it is important to further extend the two-phase model into 3D for modeling of grouts propagation in 3D fractured rocks in the future.

9. A SHORT NOTE FOR DESIGNERS

In this report, we analyzed the two solutions for radial flow of Bingham fluid (grout) between parallel disks, which is the basic theory for the RTGC method for design of rock grouting. According to the analysis results, the following notes are suggested for rock grouting designers:

- We recommend using the solution including the evolution of injected grout volume presented in this report for design of rock grouting in practice for simplicity.
- In application of RTGC method for design of rock grouting, for the 2D radial flow case, by given the following parameters:

  Hydraulic aperture 2B;

  Grouting pressure P_g;

  Groundwater pressure P_w;

  Borehole radius r_0;

  Plastic viscosity of the grout μ;

  Yield stress of the grout τ_0;

  The maximum penetration length I_{max} can be obtained by

$$I_{max} = \frac{B(P_g - P_w)}{\tau_0}$$

  The relative propagation length I_D is defined as

$$I_D = \frac{I}{I_{max}} = \frac{\tau_0(r_g - r_0)}{B(P_g - P_w)} = \frac{z_p}{B}$$

  The relative propagation length I_D can be calculated by numerical integration of the equation:

$$\frac{dt_D}{dI_D} = \frac{(I_D + 1/\gamma)\ln(I_D\gamma + 1)}{(2 - 3\,I_D + {I_D}^3)}$$

  where t_D is a dimensionless time defined as

$$t_D = t/t_0 = \frac{t{\tau_0}^2}{6\mu(P_g - P_w)}, \quad t_0 = \frac{6\mu(P_g - P_w)}{{\tau_0}^2}$$

  and γ is a parameter defined as

$$\gamma = \frac{I_{max}}{r_0} = \frac{B(P_g - P_w)}{r_0 \tau_0}$$

The evolution of grouting flowrate Q_g can be determined by

$$Q_g = \frac{2I_D + 2/\gamma}{1 + 2/\gamma} \cdot \frac{(2 - 3\,I_D + {I_D}^3)}{(I_D + 1/\gamma) ln\,(I_D\gamma + 1)} \cdot \frac{V_{g,max}}{t_0}$$

where $V_{g,max}$ is the maximum injection volume can be calculated by

$$V_{g,max} = 2\pi B {I_{max}}^2 (1 + 2/\gamma)$$

The evolution of grouting flowrate Q_g can be used in the determination of stop time for the injection once a limited flowrate value is accepted as the stop criteria.

- When the grout viscosity is below 25 mPa, it is suggested applying the two-phase flow model to consider the groundwater flow (displaced by injected grouts) during the grouting process; otherwise, it may overestimate the penetration length more than 20 % in the 1D channel flow case.
- The analytical solutions based on a single fracture can be used for parameter scoping in the design. However, it is better to apply discrete fracture networks modeling results for the design of rock grouting since complex fracture networks rather than single fractures exist in natural rock masses in reality.
- Rock characterization by hydraulic tests and grout properties characterization in real-time are important for prediction of rock grouting since fracture network structures, hydraulic aperture variability and grout properties are all important design parameters that can affect grout propagation rate. The more accurate of these parameters will help to minimize the potential uncertainty in modeling of rock grouting for the design.

10. REFERENCES

Bahman B, Skjølsvold O, Justnes H, Olsson R, Grøv E, Aarset A, 2019, Cements for tunnel grouting – Rheology and flow properties tested at different temperatures, Tunnelling and Underground Space Technology, Volume 91, 2019, 103011,ISSN 0886-7798, https://doi.org/10.1016/j.tust.2019.103011.

Baghbanan A, Jing L, 2007, Hydraulic properties of fractured rock masses with correlated fracture length and aperture, International Journal of Rock Mechanics and Mining Sciences, 44(5): 704-719.

Barnes H. 1999, The yield stress—a review or 'πανταρει'—everything flows? J. Non-Newton. Fluid Mech. 81:133–78.

Bird, RB., Stewart W. and Lightfoot E., 1960 Transport Phenomena, John Wiley & Sons, New York.

Cacas, M. C., Ledoux, E., Marsily, G., Tillie, B., Barbreau, A., Durand, E., Feuga, B., and Peaudecerf, P. (1990), Modeling fracture flow with a stochastic discrete fracture network: calibration and validation: 1. The flow model, Water Resour. Res., 26(3), 479– 489, doi:10.1029/WR026i003p00479.

Cvetkovic V., and Frampton, A., 2012. Solute transport and retention in three-dimensional fracture networks, Water Resour. Res., 48: 2, W02509. https://doi.org/10.1029/2011WR011086

Dai G, Bird B, 1981, Radial flow of a Bingham fluid between two fixed circular disks. Journal of Non-Newtonian Fluid Mechanics, 8:349-355.

Deng, S., Wang, X., Yu, J. et al., Simulation of Grouting Process in Rock Masses Under a Dam Foundation Characterized by a 3D Fracture Network, Rock Mech Rock Eng. 51: 1801. https://doi.org/10.1007/s00603-018-1436-y

Dershowitz, W., D. Shuttle, G. Lee, and S. Rogers, 2007, Analysis of Groundwater Inflow Control by Grouting Using the Discrete Fracture Network Method. Felsbau, 2007; 25(4): 34-41.

Dreuzy, J.-R., Méheust, Y., and Pichot, G. (2012), Influence of fracture scale heterogeneity on the flow properties of three-dimensional discrete fracture networks (DFN), J. Geophys. Res., 117, B11207, doi:10.1029/2012JB009461.

Dverstop B., J. Andersson, Application of the discrete fracture network concept with field data: possibilities of model calibration and validation, Water Resour Res, 1989; 25 (3): 540-550.

El Tani M (2012) Grouting Rock Fractures with Cement Grout. Rock Mechanics and Rock Engineering 45:547–561. doi: 10.1007/s00603-012-0235-0

El Tani M, Grouting emancipation. The Grout Line, 2013; 32-38.

El Tani, Grout—time to break through the SL dispute. Geotech News, 2009; 27(3):41–

49.

Emmelin A, Brantberger M, Eriksson M, Gustafson G, Stille H, 2007 Rock grouting: current competence and development for the final repository, SKB Report, R-07-30.

Eriksson M., H. Stille, J. Andersson, 2000 Numerical calculations for prediction of grout spread with account for filtration and varying aperture, In Tunnelling and Underground Space Technology, 15(4): 353-364.

Fidelibus C and Lenti V. 2012 The propagation of grout in pipe networks. Computers & Geosciences. 45:331-336.

Frampton A, Hyman JD, Zou L 2019, Advective transport in discrete fracture networks with connected and disconnected textures representing internal aperture variability,Water resources research 55 (7), 5487-5501.

Funehag J, Thörn J, Fundamentals around grouting and penetration of grout. In: Proceedings of the Rock Mechanics Meeting - Rock Engineering Research Foundation, 2014; 105–114.

Funehag J., Å. Fransson, 2006, Sealing narrow fractures with a Newtonian fluid: Model prediction for grouting verified by field study, Tunnelling and Underground Space Technology, 21(5): 492-498.

Funehag Johan, Johan Thörn, 2018, Radial penetration of cementitious grout – Laboratory verification of grout spread in a fracture model, Tunnelling and Underground Space Technology, Volume 72, 2018, Pages 228-232.

Ghafar, A., Sadrizadeh, S., Magakis, K., Draganovic, A., and Larsson, S. 2017 Varying Aperture Long Slot (VALS), a Method for Studying Grout Penetrability into Fractured Hard Rock, Geotechnical Testing Journal, Vol. 40, No. 5, pp. 871-882,

Gustafson G, Claesson J, Fransson Å (2013) Steering Parameters for Rock Grouting. Journal of Applied Mathematics. doi: 10.1155/2013/269594

Gustafson G, Claesson J, Steering parameters for rock grouting. Unpublished paper, submitted to International Journal of Rock Mechanics and Mining Science, 2005.

Gustafson G, Stille H, Stop criteria for cement grouting, Felsbau, 2005; 25:62–68.

Hoang VT, Liu WK, Park JM. 2021, Discussion on “Analysis of Bingham fluid radial flow in smooth fractures” [J. Rock Mech. Geotech. Eng. 12 (2020) 1112–1118], J. Rock Mech. Geotech. Eng., 13 (4).

Hässler L. 1991 Grouting of Rock—Simulation and Classification. Ph.D. Thesis, Dept. of Soil and Rock Mechanics, Royal Institute of Technology, Stockholm, Sweden.

Hässler, L., Håkansson , U., Stille, H. 1992 Computer-simulated flow of gorut in jointed rock. Tunneling and underground space technology, 7(4), pp. 441-446.

Håkansson U. 1987 Modellförsök – Icke-Newtonsk strömning i endimensionella

kanaler. [Master Thesis].Department of Civil and Environmental Engineering, KTH Royal Institute of Technology, Stockholm, Sweden.

Håkansson U 1993 Rheology of fresh cement based grouts. PhD Thesis, Royal Institute of Technology, Stockholm, Sweden.

Håkansson, U., Hässler, L., Stille, H. 1992 Rheological properties of microfine cement grout. Tunneling and underground space technology, 7(4), pp. 453-458.

Jin L, Sui W, Xiong J. 2019. Experimental Investigation on Chemical Grouting in a Permeated Fracture Replica with Different Roughness. Appl. Sci. 9(13): 2762.

Kobayashi S, Stille H, Gustafson G, Stille B, Real time grouting control method: development and application using Äspö HRL data. R-08-133, Swedish Nuclear Fuel and Waste Management Company, Stockholm, Sweden, 2008.

Li S, R Liu, Q Zhang, X Zhang, 2016, Protection against water or mud inrush in tunnels by grouting: A review, Journal of Rock Mechanics and Geotechnical Engineering, 8(5): 753-766.

Liang Y, W Sui, J Qi, 2019, Experimental investigation on chemical grouting of inclined fracture to control sand and water flow, Tunnelling and Underground Space Technology, 83: 82-90.

Lipscomb GG, Denn MM, Flow of Bingham fluids in complex geometries. J Non-Newtonian Fluid Mech., 1984; 14:337–346.

Lombardi G. 1985, The role of cohesion in cement grouting of rock. Commission Internationale, Lusanne, Switzerland.

Long J.C.S., J.S. Remer, C.R. Wilson, P.A. Witherspoon, Porous media equivalents for networks of discontinuous fractures. Water Resour Res, 1982;18 (3): 645-658.

Mohajerani S, A Baghbanan, G Wang, SF Forouhandeh. 2017 An efficient algorithm for simulating grout propagation in 2D discrete fracture networks. International Journal of Rock Mechanics and Mining Sciences. 98:67-77.

Muravleva L. 2017, Axisymmetric squeeze flow of a viscoplastic Bingham medium. Journal of Non-Newtonian Fluid Mechanics, 249:97–120.

Nguyen V.H., S. Rémond, J.L. Gallias, J.P. Bigas, P. Muller, 2006 Flow of Herschel–Bulkley fluids through the Marsh cone, Journal of Non-Newtonian Fluid Mechanics, 139: 128-134.

Papanastasiou T.C., Flow of materials with yield, J. Rheol., 31 (1987) 385-404.

Pyrak-Nolte L.J., C.D. Montemagno, D.D. Nolte, Volumetric imaging of aperture distributions in connected fracture networks, Geophys Res Lett, 1997; 24 (18) : 2343-2346.

Rafi J., Stille H., Control of rock jacking considering spread of grout and grouting pressure. Tunnelling and Underground Space Technology, 2014; 40: 1-15.

Rafi JY, Stille H, Applicability of using GIN method, by considering theoretical approach of grouting design. Geotech Geol Eng., 2015; 33(6):1431–1448.

Rahman M, Håkansson U, Wiklund J 2015 In-line rheological measurements of cement grouts: Effects of water/cement ratio and hydration, Tunnelling and Underground Space Technology, Volume 45, January 2015, Pages 34-42, ISSN 0886-7798,

Renshaw C.E., J.C. Park, Effect of mechanical interactions on the scaling of fracture length and aperture, Nature, 1997; 386: 482-484.

Shamu TJ, Håkansson U, 2019, Rheology of cement grouts: On the critical shear rate and no-slip regime in the Couette geometry, Cement and Concrete Research, 2019, ISSN 0008-8846, https://doi.org/10.1016/j.cemconres.2019.05.014.

Stille B, Stille H, Gustafson G, Kobayashi S, Experience with the real time grouting control method. Geomech Tunnelling, 2009;2(5):447–459.

Stille H, Gustafson G, Hassler L, Geotech Geol Eng., 2012; 30:603. doi:10.1007/s10706-012-9512-7.

Stille H. 2015, Rock Grouting: Theories and Applications. Vulkan Förlag

Sui W, J Liu, W Hu, J Qi, K Zhan, 2015, Experimental investigation on sealing efficiency of chemical grouting in rock fracture with flowing water, Tunnelling and Underground Space Technology, 50: 239-249.

U.S. Army Corps of Engineers, 2014. Drilling in Earth Embankment Dams and Levees. U.S. Army Corps of Engineers, Washington, DC, USA.

Wallner M, Propagation of Sedimentation Stable Cement Pastes in Jointed Rock. Rock Mechanics and Waterways Construction, University of Aachen, BRD, 1976.

Wang, J. S. Y., T. N. Narasimhan, and C. H. Scholz 1988, Aperture correlation of a fractal fracture, J. Geophys. Res., 93(B3), 2216–2224, doi: 10.1029/JB093iB03p02216.

Warner, J., 2004. Practical Handbook of Grouting: Soil, Rock, and Structures. John Wiley & Sons, Hoboken, NJ, USA.

Zhang D, Fang Q, Lou H, Grouting techniques for the unfavorable geological conditions of Xiang'an subsea tunnel in China, Journal of Rock Mechanics and Geotechnical Engineering, 2014; 6(5): 438-446.

Zhang Q, L. Zhang, R. Liu, S. Li, Q. Zhang, 2017, Grouting mechanism of quick setting slurry in rock fissure with consideration of viscosity variation with space, Tunnelling and Underground Space Technology, 70:262-273.

Zhang W., Li, S., Wei, J. et al. Grouting rock fractures with cement and sodium silicate grout, Carbonates Evaporites, 2018; 33: 211. https://doi.org/10.1007/s13146-016-0332-3

Zhao Z., Li B., Jiang Y. 2014. Effects of fracture surface roughness on macroscopic

fluid flow and solute transport in fracture networks. Rock Mechanics and Rock Engineering. 47: 2279-2286.

Zou L, Cvetkovic V, Jing L. 2014. Roughness decomposition and effects on fluid flow in single rock fractures. The proceeding of the 8th Asian Rock Mechanics Symposium: Rock Mechanics for Global Issues- Natural Disasters, Environment and Energy, 14-16, October 2014, Sapporo, Japan.

Zou L, Håkansson U, Cvetkovic V, 2018, Modeling of rock grouting in saturated variable aperture fractures, In: Proceedings of Bergdagarna 2018, Stockholm, Sweden, 2018.

Zou L, Håkansson U, Cvetkovic V. 2020, Analysis of Bingham fluid radial flow in smooth fractures, Journal of Rock Mechanics and Geotechnical Engineering, Volume 12, Issue 5, October 2020, Pages 1112-1118.

Zou L, Håkansson U, Cvetkovic V. 2021, Reply to Discussion on 'Analysis of Bingham fluid radial flow in smooth fractures', Journal of Rock Mechanics and Geotechnical Engineering, 13 (4) https://doi.org/10.1016/j.jrmge.2021.04.001

Zou L, Håkansson U, Cvetkovic V. 2020, Yield-power-law fluid propagation in water-saturated fracture networks with application to rock grouting, Tunnelling and Underground Space Technology, Volume 95, January 2020, 103170.

Zou L, Håkansson U, Cvetkovic V, 2020, Radial propagation of yield-power-law fluids into water-saturated homogeneous fractures with application to rock grouting, Volume 130, June 2020, 104308. https://doi.org/10.1016/j.ijrmms.2020.104308.

Zou L, Håkansson U, Cvetkovic V. 2019, Cement grout propagation in two-dimensional fracture networks: Impact of structure and hydraulic variability. International Journal of Rock Mechanics and Mining Sciences. 115: 1-10.

Zou L, Håkansson U., Cvetkovic V. 2018, Two-phase cement grout propagation in homogeneous water-saturated rock fractures. International Journal of Rock Mechanics and Mining Sciences, 106: 243–249.

Zou L, Håkansson U, Cvetkovic V. 2019, Cement grout propagation in 2D fracture networks: impact of rheology, the 14th ISRM congress, September 13-18, 2019, Foz do Iguaçu, Brazil.

Zou L, Håkansson U, Cvetkovic V. 2019, Non-newtonian grout flow in single rough-walled rock fractures, Bergdagarna 2019. March 19, 2019, Stockholm.

Zou L, Håkansson U, Cvetkovic V. 2018, Impacts of Elastic Jacking on Rock Grouting, In Proceeding of the 10th Asian Rock Mechanics Symposium, 29 October to 03 November 2018, Singapore.

Zou L, Jing L., Cvetkovic V. 2016, Assumptions of the analytical solution for solute transport in a fracture-matrix system. International Journal of Rock Mechanics and Mining Sciences, 83: 211–217.

Zou L, Jing L., Cvetkovic V. 2015, Roughness decomposition and nonlinear fluid flow

in a single rock fracture. International Journal of Rock Mechanics and Mining Sciences. 75: 102-118.

Zou L, Jing L., Cvetkovic V. 2017a, Modeling of solute mixing at 3D rough-walled fracture intersections. Advances in Water Resources, 107, 1-9.

Zou L, Jing L., Cvetkovic V. 2017b, Shear enhanced nonlinear flow in rough-walled rock fractures. International Journal of Rock Mechanics and Mining Sciences, 97: 33-45.

BeFo

Box 55545
SE-102 04 Stockholm

info@befoonline.org • www.befoonline.org
Visiting address: Sturegatan 11, Stockholm

ISSN 1104-1773